Escola Tècnica Superior d'Enginyeria de Telecomunicació de Barcelona

UNIVERSITAT POLITÈCNICA DE CATALUNYA

Optimal deployment of UAV based Mobile Base Stations in emergency scenarios

by

David Grau Marina

A Master's Thesis submitted to the Faculty of the
Escola Tècnica Superior d'Enginyeria de Telecomunicació de Barcelona,
Universitat Politècnica de Catalunya

Advisors

Dr. Toktam Mahmoodi

Dr. Anna Umbert

In partial fulfillment of the requirements for the
Master's Degree in Telecommunications Engineering

London, July 2019

Abstract

In emergency scenarios where ground base stations are no longer available, Unmanned aerial vehicles (UAVs) based mobile base stations (MBS) can provide a good solution to provide coverage to the ground terminals in the affected area thanks to their versatility and affordability. The objective of this work is to study how these MBS can be deployed in the affected area minimizing the number of devices deployed at the same time than maximizing the coverage of every single user. We based our placement on an spiral algorithm path from the edge users towards the area center by minimizing the power consumption of each device and the interference in the MBS network. Once the MBS is already placed, we optimized the power consumption by making use of multi-antenna techniques to generate directional beams introducing the Non-Orthogonal Multiple Access (NOMA) technique, a promising technology in the upcoming fifth generation (5G). Finally, numerical results show how our algorithm improves the performance of the previous one in terms of quality of service (QoS) of the ground user.

Resumen

En escenarios imprevistos donde la estación base terrestre deja de estar disponible, estaciones bases móviles (MBS) montadas en *Unmanned aerial vechicles* (UAVs) pueden suponer una buena solución para proveer cobertura a los terminales móviles dentro del área afectada debido a su versatilidad y a su precio cada vez más asequible. El objetivo de este trabajo es estudiar como se puede desplegar una red de MBS en el área afectada minimizando el número de UAV utilizados, a la vez de maximizar la cobertura de cada uno de los usuarios. El posicionamiento de las MBS se ha basado en un algoritmo en espiral cubriendo primero los usuarios de los bordes hacia los del centro del área afectada, minimizando el consumo de energía de cada dispositivo independientemente, a la vez de la interferencia que se puede producir en la red de MBS lanzadas. Una vez el MBS ha sido colocado en un punto tridimensional, el consumo de energía ha sido mejorado haciendo uso de técnicas multi-antena para generar un haz direccional. Para ello se ha hecho uso de la técnica conocida como *Non-Orthogonal Multiple Access* (NOMA), una tecnología muy prometedora para la venidera quinta generación (5G) móvil. Finalmente, se muestran una serie de resultados mostrando como nuestro algoritmo mejora las prestaciones de la versión anterior en cuanto a la calidad de servicio (QoS) del destinatario final.

Resum

A escenaris en situacions imprevistes on la estació base terrestre deixa d'estar disponible, estacions bases mòbils (MBS) muntades en *Unmanned aerial vechicles* (UAVs) poden suposar una bona solució per proveir cobertura als terminals mòbils dins de l'àre afectada gràcies a la seva versatilitat i al seu preu cada com més assequible. L'objectiu d'aquest treball és estudiar com es pot desplegar una xarxa de MBS a l'àrea afectada minimitzant el nombre de UAV utilitzats, d'igual forma tractant de maximitzar la cobertura de cada un dels usuaris. El posicionament de les MBS s'ha basat en un algorisme en espiral que cobreix primer els usuaris dels extrems cap als usuaris del centre de l'àre afectada, minimitzant el consum d'energia de cada dispositiu independentment, així com la interferència que es pot produir a la xarxa de MBS llançats. Un cop les MBS han estat situades en un punt tridimensional, el consum d'energia ha sigut millorat fent ús de tècniques multi-antena per generar un feix direccional. S'ha fet ús de la tècnica coneguda com *Non-Orthogonal Multiple Access* (NOMA), una tecnologia molt prometedora per la inminent cinquena generació (5G) mòbil. Finalment, es mostren una sèrie de resultats que mostren com el nostre algorisme millora les prestacions de la versió anterior pel que fa a la qualitat del servei (QoS) del destinatari final.

Acknowledgements

This works concludes a long and important stage in my life. This is a full stop in a six years path with intense work and dedication. Thanks to my studies, I have been able to discover a whole world full of innovation.

First of all, I would like to thank the advisor of my thesis, Dr. Toktam Mahmoodi, for giving me the opportunity to join King's College and move to the amazing and cosmopolitan city of London. I would also thank my co-advisor in Barcelona for supervising the project in the distance. Last but not least, I want to thank my nearby family and my girlfriend. They have given me support in every single moment, in the good ones and the tough as well.

List of Figures

Contents

1 Introduction

1.1 Project Outline

This thesis study the optimal deployment of MBS in emergency scenarios, where some special conditions such as maximum coverage have to be fulfilled. The scope of this project is to set up a solid work in this area.

1.1.1 Requirements and Assumptions

The development of this project is described in the following lines. In order to make an accurate study of the deployment problem, the work has been basically broken down into four main work-packages:

- Problem statement: in this starting point, it was required to get some knowledge about the previous work done in UAV mounted Mobile Base Stations deployment and communications.
- Scenario description: it is necessary to define a certain system model to follow during the work, as well as introduce some useful nomenclature. Moreover, the propagation model in the scenario need to be studied in order to define the path losses affected within the link.
- Placement algorithm: this is the core of the work. It is required to identify, study and implement an optimal placement algorithm in terms of MBS deployment.
- ATG communication: beyond the placement, it is mandatory to study the communication link between the MBS and the GT in this scenario.
- Results validation: it is mandatory to verify simulations and algorithm results. Moreover, simulations back up theoretical study and conclude the validity of the theories.

Further information about time planning and realization of the different work-packages is shown in appendix A, including the Gantt diagram.

1.2 Organization

This master's thesis have six chapters, while the main work can be found in chapters three, four and five. The first one, chapter 1, includes the introduction of the work, where the project scopes and requirements are analyzed. This chapter presents the structure of the project. The second one, chapter 2, introduces and reference the staring point of the project, as well as review the literature with similar works.

In chapter 3 we introduce the system model followed during the thesis, as well as the propagation model used in the MBS deployment. Chapter 4 present the core of the work, consisting on the placement optimization problem. Results are presented demonstrating the performance of the algorithm in our scenario. In chapter 5 we approach the problem of multi-user communications in ATG communications by using a novel technique called NOMA.

Finally, chapter 6 includes the conclusions and future tasks in order to make a complete analysis of the topics developed in this thesis.

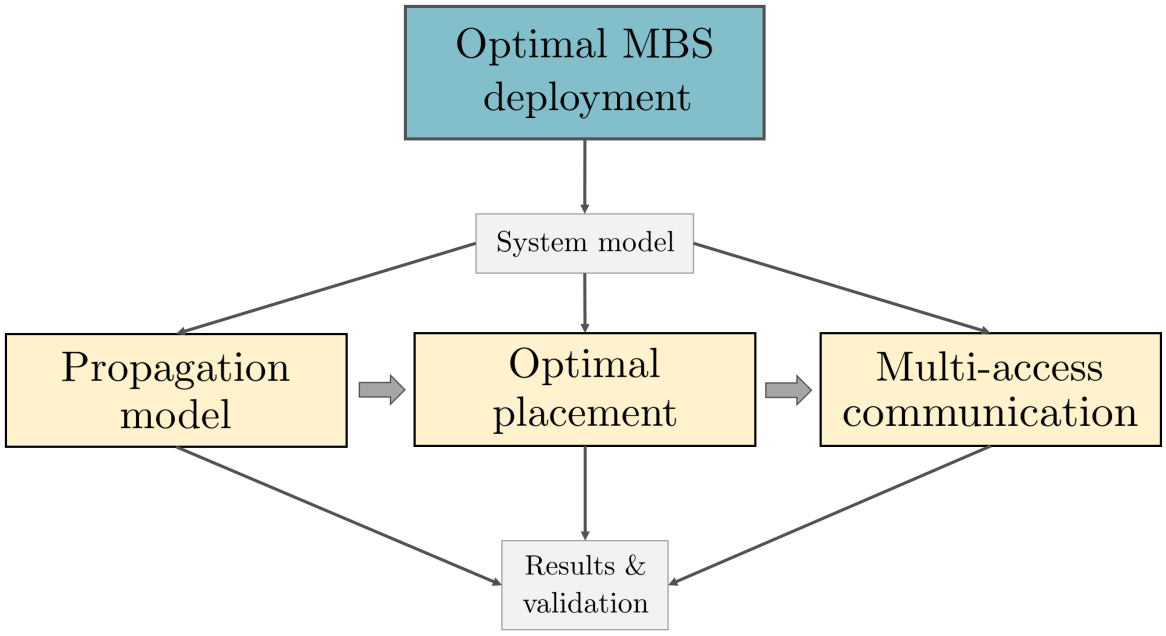

Figure 1.1: Master's thesis structure.

2 State of the art

Unmanned aerial vehicles (UAVs), in special drones, are gaining a lot of popularity thanks to their versatility and affordability. They offer a promising solution in wireless services thanks to their rapid deployment [1]-[2]. In particular, UAV mounted mobile base stations (MBSs) have found a wide range of applications, such as offloading traffic from a congested terrestrial base stations (TBSs) or provide wireless connectivity in emergency scenarios such as disaster scenes or areas when the TBS are no longer available due to some malfunction [3]-[4].

A proper communication network is essential in emergency scenarios when the ground infrastructure is damaged. UAV communications is being a hot topic in the recent times, but there is few work focusing on how this devices can be useful in emergency scenarios. MBS can provide temporary coverage while the affected ground infrastructure is fixed. Many of the work focus the MBS deployment to offload TBS in demanding scenarios, such as music concerts or sports events, when a larger amount of GTs is expected for a certain amount of time. However, there is not much research in the deployment when the TBS is down [5].

MBS can be placed in any location, and their trajectory is only constrained by physical characteristics, so they are suitable to cover ground terminals (GTs) in a given area. Despite their promising benefits, UAV based communications are facing many challenges. Unlike terrestrial links, where the location of the TBS is fixed, so that the path losses are depending on the location of the ground user, the air-to-ground (ATG) channels are a function of the location of the GT and the MBS as well [6].

A key challenge in UAV based communications is the MBS placement. Moreover, this placement is not a two dimensional problem anymore, it is now a three dimensional problem. Moreover, the power budget available for the onboard electronics is very limited because of the battery life [7]-[8]. Then, it is quite important to optimize the MBS placement to reduce the impacts of that drawbacks. Authors in [9] study the three dimensional placement of a single MBS to offload as many GTs as possible from the TBS by maximizing the coverage with different QoS requirements. Authors in [10] reproduce a similar problem by placing a single

MBS minimizing the power consumption by adjusting the coverage radius to serve the edge user. Authors in [11] extended the placement problem to multiple MBS to cover a certain area by minimizing the deployment costs, and they propose an spiral algorithm to place the MBS network. In this work we try to solve the deployment problem by maximizing the coverage in emergency scenarios, where no TBS are available. We improve the work in [11] by constraining the problem to realistic conditions and minimizing the described drawbacks.

We assume that the GT locations are known and the MBSs are flying at a fixed altitude. We focus the MBS placement problem to provide coverage for all GTs in the affected area by minimizing the power consumption and the interference between MBSs. This deployment is intended to be used in emergency scenarios, where the QoS of each user is important and the system is intended to be as much fair as possible. The placement problem can be formulated as the Geometric Disk Cover (GDC) [12]-[13], whose objective is to cover a set of given nodes (GTs) in a region with the minimum number of disks of given radius (MBS coverage radius). This problem is NP-hard, so the computational complexity is too high. The purposed algorithm places each MBS sequentially, covering first the GTs in the area perimeter towards the GTs in the center of that area. This placement creates a path connecting the MBSs in a spiral way from outwards to indwards the area, hence the spiral algorithm name.

Finally, the deployment problem is extended beyond the placement. Non-orthogonal multiple access (NOMA) is a promising technology for the fifth generation (5G) due to its high spectral efficiency [14]. We applied this technique to the already placed drones to improve the coverage towards the GTs by making use of multi-antenna techniques [15] to generate directional beams. We show how higher data rates can be achieved rather than using (Orthogonal multiple access) OMA techniques [16], paying important attention to the interference.

3 | System model

3.1 Scenario description

We consider a cellular system where either one or some terrestrial base stations (TBS) are no longer operative due to congestion or a malfunction of the infrastructure. Therefore, a network of UAV based mobile base stations (MBS) is deployed to maintain the connectivity of the ground terminals (GT). MBSs can communicate among them, and the closest one to others operative TBS are backhaul connected to operative TBS. The scenario is depicted in Figure 3.1.

We assume an area of interest with K GTs, denoted by the set $\mathcal{K} = \{1, 2, \ldots, K\}$ at a known location $\{\mathbf{w}_k\} \in \mathbb{R}^{3\times 1}$ with $k \in \mathcal{K}$. Each location $\{\mathbf{w}_k\}$ represents the three-dimensional (3D) coordinates of the k-th GT, that is $\mathbf{w}_k = [\ \mathbf{r}_k \quad h_k\ ]^T$, where $\mathbf{r}_k$ stands for the 2D coordinates in the horizontal plane and $h_k = 0\ \ \forall k \in \mathcal{K}$. To serve the GTs, M MBSs are deployed, denoted by the set $\mathcal{M} = \{1, 2, \ldots, M\}$ at a location $\{\mathbf{u}_m\} \in \mathbb{R}^{3\times 1}$ with $m \in \mathcal{M}$. In the MBS case, each location $\{\mathbf{u}_m\}$ stands for the 3D coordinates of the m-th MBS, and can be broken down in both 2D coordinates and height in the same way than $\mathbf{w}_k$. In this scenario, the original cell covered by the damaged TBS is now divided in M micro-cells of equivalent radius R_m projected on the ground aiming to cover as many users as possible.

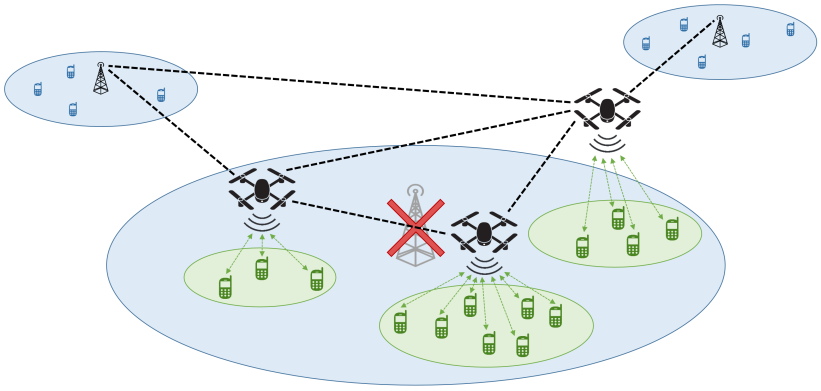

Figure 3.1: System model with an auxiliary MBS network already deployed.

3.2 Propagation model

Not many literature consider the problem of characterizing the air-to-ground (ATG) propagation model over urban environments. Some of them provide statistical models based on Line-of-Sight (LoS) conditions, while another group considers the problem of no Line-of-Sight (NLoS) with strong reflections. The model used in [6] show how ATG links can be either LoS or NLos with some probability in urban environments. Figure 3.2 depicts the scenario, where the ATG link is divided into two segments: free-space path losses segment and an additional excessive path losses segment within the urban environment. In addition, in the urban area many links may be affected by reflection, diffraction or scattering.

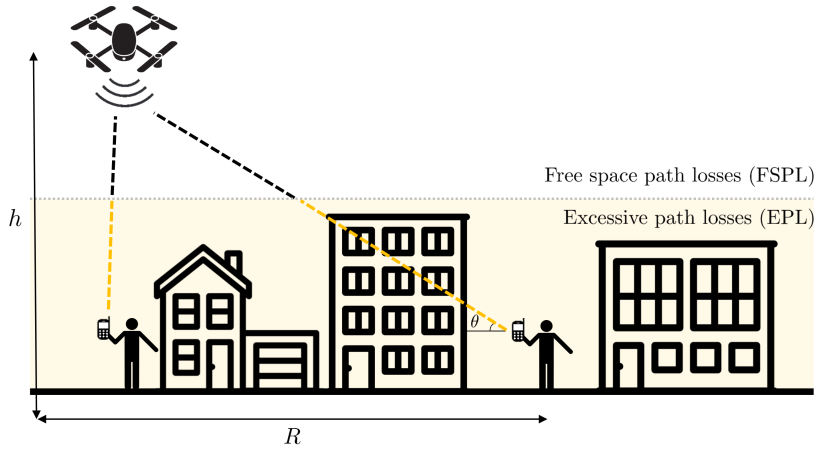

Figure 3.2: Air-to-ground propagation model in urban environments.

We can model the resulting path losses between the UAV and the ground as

$$\mathrm{PL}_\gamma = \mathrm{FSPL} + \mathrm{EPL}_\gamma \tag{3.1}$$

where FSPL stands for the free space path losses, EPL stands for the excessive path losses and $\gamma \in \{\mathrm{LoS}, \mathrm{NLoS}\}$ refers to the propagation group.

In order to find the total path losses, we apply the discrete expectation such as

$$\mathrm{PL} = \sum_{\gamma} \mathrm{PL}_\gamma \mathrm{P}(\gamma, \theta) \tag{3.2}$$

where $\mathrm{P}(\gamma, \theta)$ defines the probability of occurrence of the propagation group γ and θ is the elevation angle of the ATG link.

In our study we have set the propagation groups up to two, related to the LoS condition. Hence, the probability of each group is

$$\mathrm{P}(\mathrm{LoS}, \theta) = 1 - \mathrm{P}(\mathrm{NLoS}, \theta) \tag{3.3}$$

3.2.1 Line-of-Sight (LoS) probability model

The International Telecommunication Union (ITU) shows a possible formulation to the LoS problem between a transmitter at height h_{Tx} and a receiver at height h_{Rx} in urban environments. That model is highly dependent on three parameters related to the environment:

- Parameter α : the ratio of land area covered by buildings to total land area (dimensionless).
- Parameter β : the mean number of buildings per unit area (building/km^2).
- Parameter γ : a variable determining the building height distribution according to Rayleigh probability distribution: $P(h) = (h/\gamma^2)\exp(-h^2/2\gamma^2)$, where h is the building height in meters.

Given α, β and γ, the LoS probability can be written [6] as

$$\mathrm{P}(\mathrm{LoS}) = \prod_{b=1}^{B} \mathrm{P}(h_b < h_{LoS}) \tag{3.4}$$

where B is the number of buildings crossed by the LoS ray and

$$h_{LoS} = h_{Tx} - \frac{d_{LoS}(h_{Tx} - h_{Rx})}{d_{TxRx}} \tag{3.5}$$

where h_{Tx} is the height above ground of the transmitter, h_{Rx} is the height of the receiver at the distance d_{TxRx} and d_{LoS} is the distance from the transmitter to the obstacle. After some mathematical steps in [**?**] we get a single expression for the LoS probability as

$$\mathrm{P}(\mathrm{LoS}) = \prod_{b=1}^{B} \left[1 - \exp\left(- \frac{\left(h_{Tx} - \frac{(b + 1/2)(h_{Tx} - h_{Rx})}{B} \right)^2}{2\gamma^2} \right) \right] \tag{3.6}$$

where the number of buildings can be written as $B = \lfloor d_{TxRx} \cdot b_{km} \rfloor$ and $b_{km} = \sqrt{\alpha\beta}$ is the expected number of buildings passed per km.

For the sake of simplicity, in our scenario we are considering $h_{Tx} = h_m$, which stands for the height of the m-th MBS, and $h_{Rx} = h_k = 0$ for all GTs. Hence, the projected ground distance becomes $r_{mk} = h_m / \tan(\theta_k)$.

Environment	**Parameter** α	**Parameter** β	**Parameter** γ
Sub-urban	0.1	750	8
Urban	0.3	500	15
Dense-urban	0.5	300	20
High-rise-urban	0.5	300	50

Table 3.1: Line-of-sight parameters for different urban environments.

Table 3.1 resumes the list of parameters defining each of the different urban environments used to depict the LoS probability in figure 3.3 in terms of the elevation angle θ. Resulting probabilities can be closely approximated to a simple modified Sigmoid function (S-curve), which simplifies the calculation of the LoS probability, formulated as:

$$\mathrm{P}(\mathrm{LoS}, \theta) = \frac{1}{1 + a \exp(-b[\theta - a])} \tag{3.7}$$

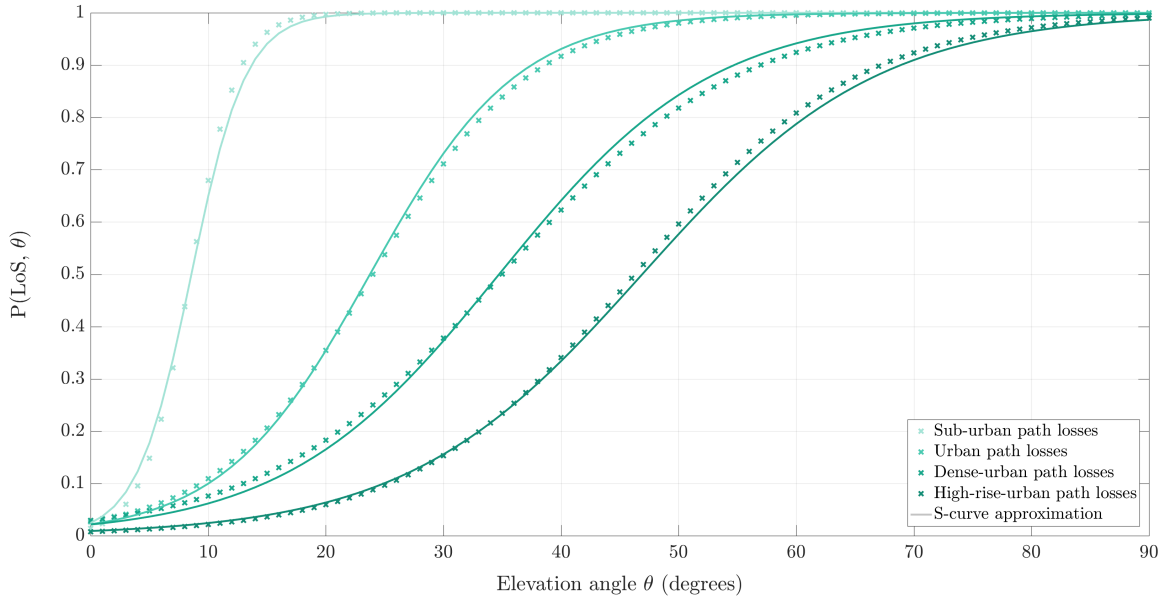

Figure 3.3: Line-of-sight probabilities for different urban environments.

Figure 3.3 shows the LoS probabilities for each environment in terms of the elevation angle θ, with the related S-curve approximation. The resulting probability is monotonically increasing, achieving its maximum when the MBS is above the GT, that is $\theta = 90°$. If the environment is plenty of obstacles such as big buildings, which may produce shadowing and scattering, the probability to get a LoS ray becomes more unlikely.

3.2.2 Path losses

Once we know the expressions for LoS and NLos probabilities, we need to focus to the path losses of both propagation pair. We can rewrite (3.1) according to Friis equation as

$$\begin{aligned} \mathrm{PL}_{\mathrm{LoS}} &= 20\log\left(\frac{4\pi f_c d_{mk}}{c}\right) + \eta_{\mathrm{LoS}} \\ \mathrm{PL}_{\mathrm{NLoS}} &= 20\log\left(\frac{4\pi f_c d_{mk}}{c}\right) + \eta_{\mathrm{NLoS}} \end{aligned} \tag{3.8}$$

where f_c is the carrier frequency, d_{mk} is the distance in the three dimensional domain between the m-th MBS and the k-th GT given by $d_{mk} = \sqrt{h_m^2 + r_{mk}^2}$ and η_γ is related to the excessive path losses of both propagation scenarios. Then, from (3.2) we have

$$\mathrm{PL} = \mathrm{P(LoS)} \times \mathrm{PL}_{\mathrm{LoS}} + \mathrm{P(NLoS)} \times \mathrm{PL}_{\mathrm{NLoS}} \tag{3.9}$$

From figure 3.2 we can rewrite the elevation angle as $\theta_k = \arctan(h_m/r_{mk})$. Substituting (3.7) and (3.8) into (3.9) and performing some algebraic reductions, we get

$$\mathrm{PL} = \frac{A}{1 + a\exp\left(-b\left[\arctan\left(\frac{h_m}{r_{mk}}\right) - a\right]\right)} + 10\log(h_m^2 + r_{mk}^2) + B \tag{3.10}$$

where $A = \eta_{\mathrm{LoS}} - \eta_{\mathrm{NLoS}}$ and $B = 20\log(\frac{4\pi f_c}{c}) + \eta_{\mathrm{NLoS}}$.

3.2.3 Results and discussion

In this subsection we are going to evaluate the path losses behaviour over different conditions and different urban environments. The experiments have been developed using the values in table 3.2, which are related to the ones showed in table 3.1, to fulfill equation (3.10), and for a system frequency of $f_c = 2$ GHz.

Environment	a	b	$\eta_{\mathbf{LoS}}$	$\eta_{\mathbf{NLoS}}$
Sub-urban	4.88	0.43	0.1	21
Urban	9.61	0.16	1.0	20
Dense-urban	12.08	0.11	1.6	23
High-rise-urban	27.23	0.08	2.3	34

Table 3.2: Propagation parameters.

On the other hand, figure 3.4 shows the path losses evolution for a fixed MBS altitude of $h_m = 150$ meters for different horizontal distances. We can see how the path losses increase rapidly for small horizontal distances, and then that increment becomes much more slower and it is almost flat. This effect is produced due to the buildings density in the area. We can also see how the sub-urban path losses initially merge with free-space path losses and at the end merge with urban path-losses. This effect may be produced for some diffraction effects because of the buildings.

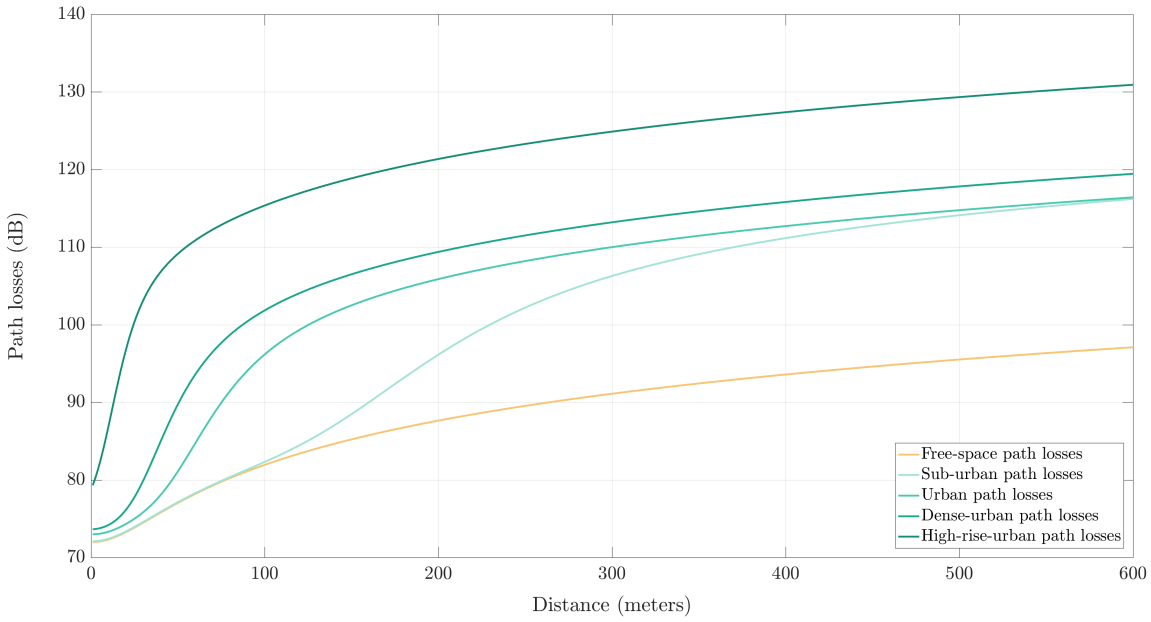

Figure 3.4: Path losses evolution in terms of MBS coverage radius.

Figure 3.5 shows the path losses evolution for a fixed coverage radius of value $R = 300$ meters for different MBS altitude values, from floor ($h_m = 0$) to 500 meters. For low altitudes different propagation effects can occur because of the height of the buildings, such as reflection,

diffraction, scattering or multipath propagation. Once the MBS altitude overtakes the mean building height, path losses hugely decrease. Keeping increasing the altitude of the MBS lead to higher path losses. In this graph we can see how there exists and optimal height value that minimizes the path losses for a certain horizontal distance and for a certain urban environment characterization.

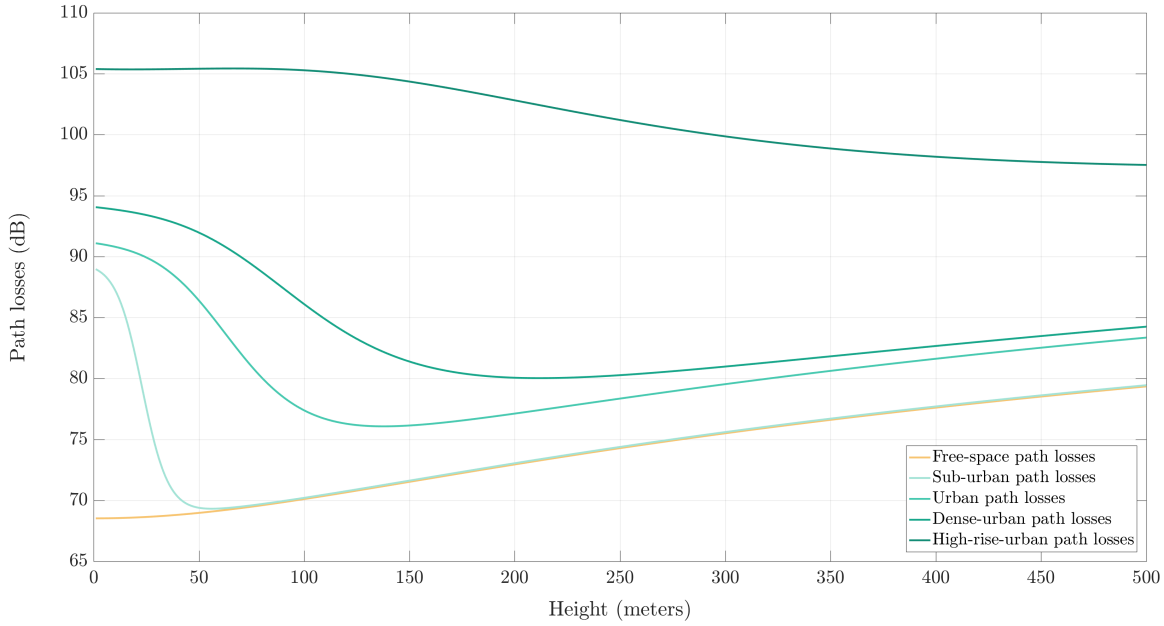

Figure 3.5: Path losses evolution in terms of MBS altitude.

In order to give some meaning to those results, we depict in figure 3.6 the variation of the MBS coverage radius with respect to the MBS altitude for each urban environment for $\mathrm{PL}_{th} = 100$ dB. As it was expected from the separated plots, higher distances are needed in the sub-urban environment to achieve that path losses threshold, while a high-rise-urban environment reaches that value rapidly. In addition, we can see how the plots have a maximum value for a certain radius and altitude. This effect can be better understood in figure 3.7, which is showing the same idea than figure 3.6 for different path losses values in a single environment, in this case a urban environment. We can notice that all the maximum values are aligned, which indicates a constant ratio between the MBS coverage radius R_m and the optimal MBS altitude $h_{m,opt}$. Hence, this leads to an optimal elevation angle

$$\theta_{opt} = \arctan\left(\frac{h_{m,opt}}{R_m}\right) \tag{3.11}$$

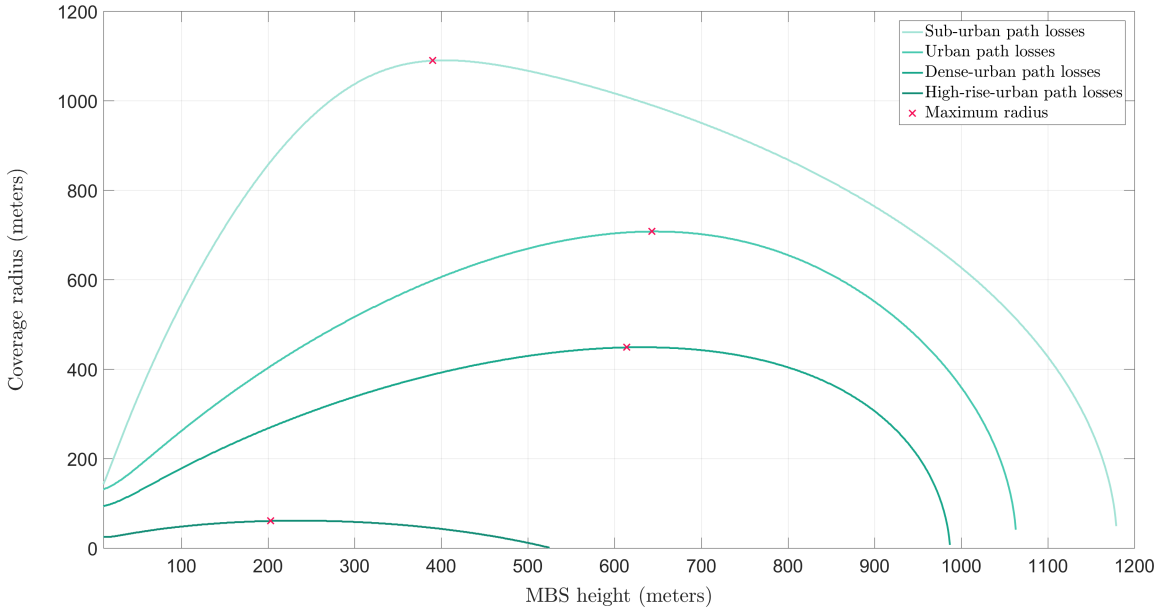

Figure 3.6: MBS radius versus altitude for different urban environments.

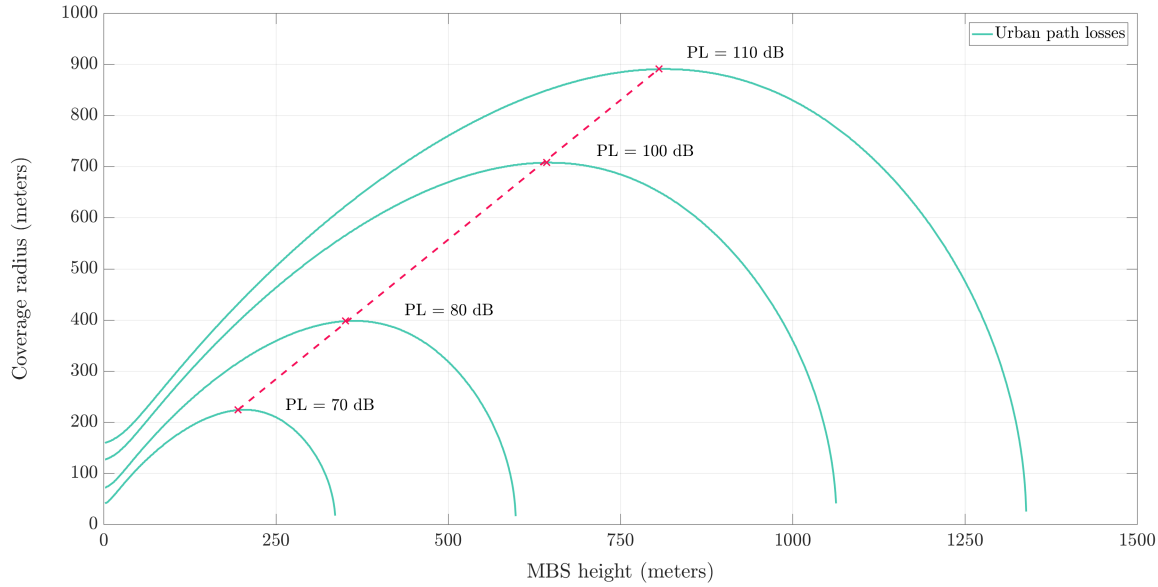

Figure 3.7: MBS radius versus altitude for different path losses.

4 | Placement optimization

In this chapter we are going to address the problem of how to optimally place the MBS network following the scenario described in 3.1. The aim of the following sections is to find the optimal position minimizing the number of MBS deployed, giving maximum coverage to every single user in the target area within some constraints. The developed algorithm is based on an spiral algorithm proposed by Lyu *et al.* in [11].

4.1 Problem statement and formulation

The placement optimization procedure has to consider some key points very important in UAV based MBS becouse of the limitations of that systems. Hence, the challenges to take into account in the algorithm are:

- **MBS positioning**: find the optimal three dimensional location for each MBS within the target area.
- **Maximum coverage**: apart to guarantee the coverage of each one of the GTs, it is important to maximize the number of GTs covered by a single MBS to reduce number of MBS deployed.
- **QoS guarantee**: apart to provide coverage, it is important to guarantee a certain quality of service to all GTs, even the edge users.
- **System life**: because of the battery limitations in this kind of vehicles, it is mandatory to minimize the MBS power consumption.
- **Cost reduction**: in terms of network, it is important to deploy the minimum number of MBS as possible to reduce the cost of the overall network.

The last challenge is the key of the algorithm. We aim to deploy the minimum number of MBS where each GT is served by any of them. Some works consider a good approach to maximize the number of GTs served for more than one MBS. In this kind of scenarios

is very important to address the inter-cell interference problem, *e.g.* proper frequency and channel scheduling, power control and channel coding. Thus, we present and algorithm trying to minimize the interference between MBS at GT level. Trying to achieve all the challenges proposed, the problem can be formulated as follows:

$$\min_{\substack{\{\mathbf{u}_m\},\ m\in\mathcal{M} \\ \{\gamma_{o,k}\},\ k\in\mathcal{K}}} \quad |\mathcal{M}| \quad \text{s.t} \quad \begin{cases} \Phi_1 : \min\limits_{m\in\mathcal{M}} \|\mathbf{w}_k - \mathbf{u}_m\| \leqslant d_m \\ \Phi_2 : r_m \leqslant R_{max} \\ \Phi_3 : \gamma_{o,k} \geqslant \gamma_{o,min} \end{cases} \tag{4.1}$$

For a better understanding of the optimization problem, we are going to break down each one of the constraints and review the notation.

- **Constraint** Φ_1: this constraint is related to the coverage maximization challenge. We try to cover as much GTs as possible with one single MBS with a distance limitation. Hence, $\|\mathbf{w}_k - \mathbf{u}_m\|$ stands for the three dimensional distance between the k-th GT and the m-th MBS and $d_m = [\,(r_m)^2 + (h_m)^2\,]^{1/2}$ stands for the minimum possible distance available for the m-th MBS to reach all the served GTs.

- **Constraint** Φ_2: this constraint is related to the system life limitation. It is mandatory to set a maximum MBS coverage radius projected on the ground related to the maximum transmitted power to reach the edge user.

- **Constraint** Φ_3: this constraint is related to the QoS guarantee challenge. In terms of coverage, we need to guarantee a certain signal-to-interference-plus-noise ratio γ_0 to the edge user.

The problem in (4.1) is related to the Geometric Disk Cover (GDC) problem [12]-[13]. Given the GTs set $\mathcal{K}$ with K GTs distributed in the plane, place the smallest MBS set with cardinality $|\mathcal{M}|$ such that for every k-th GT with $k \in \mathcal{K}$, there exists at least one m-th MBS with $m \in \mathcal{M}$ such that $d_{mk} \leqslant R$. This problem is NP-hard to solve due to the non-convex constraint Φ_1. Then, the optimal solution of (4.1) requires computational complexity of $O(M^K)$ using brute force search. This is not feasible even for small values.

4.2 Spiral algorithm

In this section we present an heuristic algorithm to solve the problem in (4.1) by placing MBS sequentially within the target area. The main idea behind this algorithm refers to the path followed in the placement. MBS are placed sequentially along the area perimeter of the remaining uncovered GTs. This perimeter is defined by a path connecting the boundary GTs as the convex hull of all the uncovered GTs. Following this criteria, the placement follows an spiral path towards the center, until all GTs are covered. This algorithm is summarized in algorithm 1.

Algorithm 1 Spiral MBS placement algorithm

Input: GT set $\mathcal{K}$ at locations $\{\mathbf{w}_k\}$.

Output: MBS set $\mathcal{M}$ at locations $\{\mathbf{u}_m\}$.

procedure $\{\mathbf{u}_m, R_m\}$ = OPTIMAL_PLACEMENT($\{\mathbf{w}_k\}$, R_{max}, $\gamma_{0,min}$)
  $\mathcal{K}_U \leftarrow \mathcal{K}$. $\mathcal{K}_C = \varnothing$. $\mathcal{M} = \varnothing$. $m = 1$. ▷ Initialization
  while $\mathcal{K}_U \neq \varnothing$ **do**
    Find $\mathcal{K}_{U,b} \subseteq \mathcal{K}_U$ in CCW order.
    $\mathcal{K}_{U,in} \leftarrow \mathcal{K}_U \setminus \mathcal{K}_{U,b}$.
    if $m = 1$ **then**
      Get most boundary GT k_b. $k_b \leftarrow k_0$.
    end if
    $[\mathbf{u}_m, R_m, \mathcal{K}_{m,b}]$ = LOCAL_COVER($\{\mathbf{w}_k\}$, $\{k_0\}$, $\mathcal{K}_{U,b} \setminus \{k_0\}$). ▷ Cover boundary GTs
    $[\mathbf{u}_m, R_m, \mathcal{K}_m]$ = LOCAL_COVER($\mathbf{u}_m$, $\mathcal{K}_{m,b}$, $\mathcal{K}_{U,in}$). ▷ Cover inner GTs
    $\mathcal{K}_C \cup \mathcal{K}_m$. $\mathcal{M} \cup \{m\}$. $\mathcal{K}_U \leftarrow \mathcal{K}_U \setminus \mathcal{K}_m$. $m \leftarrow m + 1$.
    From $\mathcal{K}_{U,b} \setminus \mathcal{K}_{m,b}$, get first uncovered GT $k_0^{'}$ CCW from k_0. $k_0^{'} \leftarrow k_0$.
  end while
  return $\{\mathbf{u}_m, R_m\}$.
end procedure

Each m-th MBS has to cover at least one boundary GT k_0, and all the GTs at a distance higher than two times the maximum coverage radius R_{max} are removed from the iteration as they cannot be served as the same time as k_0 by one single MBS. Following this idea, MBS will be placed towards the area center, giving higher priority to boundary GTs. This is necessary to reduce the possibility that a MBS is serving only a single GT on the edge. Once the m-th MBS is placed, the area is reduced to the uncovered GTs. Hence, by placing each MBS counterclockwise CCW the area becomes smaller and smaller towards the center, until

all GTs are covered. In order to support the explanation of the algorithm, we can use the overview in figure 4.1 to illustrate the notation and every step.

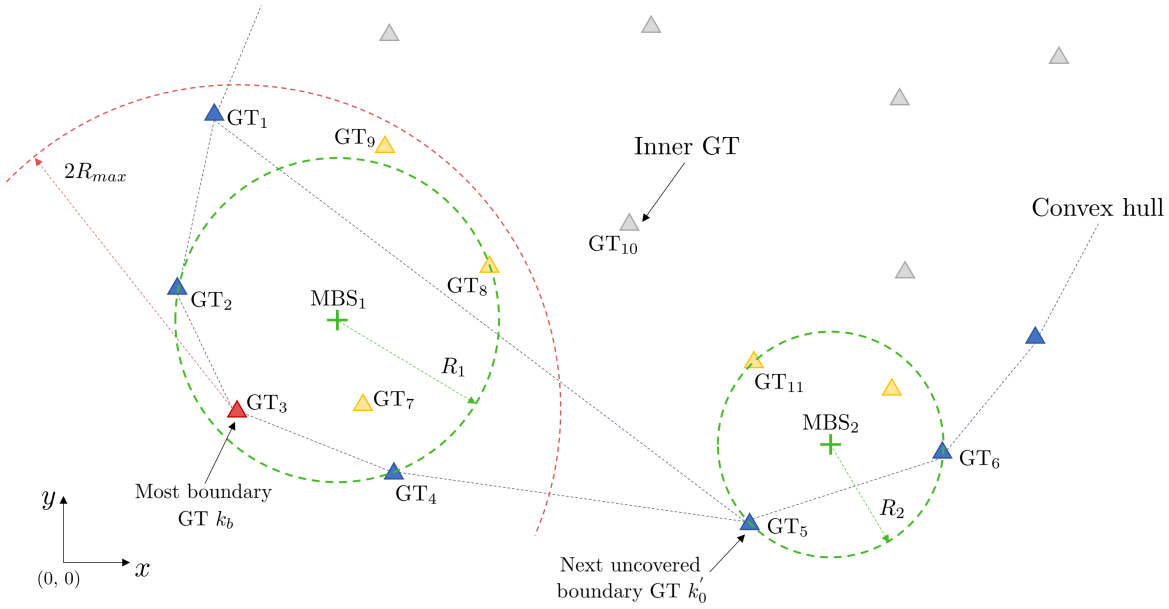

Figure 4.1: Spiral algorithm overview.

From the notation introduced in 3, let us introduce the subset of uncovered GTs as $\mathcal{K}_U \subseteq \mathcal{K}$, which is initialized to $\mathcal{K}$ at the beginning of the spiral algorithm, and $\mathcal{K}_C \subseteq \mathcal{K}$, which is empty. The uncovered GTs subset $\mathcal{K}_U$ can be divided into two groups: inner GTs $\mathcal{K}_{U,in}$, depicted as yellow triangles, and boundary GTs $\mathcal{K}_{U,b}$, depicted as dark blue triangles. Boundary GTs are listed in CCW order (step 4 in algorithm 1), which following the example results as $\mathcal{K}_{U,b} = \{1, 2, 3, 4, 5, 6, \dots\}$. In addition, note that the relation between sets can be written as $\mathcal{K}_{U,in} = \mathcal{K}_U \setminus \mathcal{K}_{U,b}$ (step 5 in algorithm 1). The criteria used to determine those boundary GTs was the convex hull, which is the smallest convex polygon that encloses all of the points in the set. This can be easily done by applying the rubber band analogy [13]. In the algorithm we give higher priority to the boundary GTs to increase the coverage of each MBS. In this sense, it is guaranteed that a subset of the boundary GTs is covered by each iteration of the algorithm, that is a new MBS placement.

To place the first MBS we select the most boundary GT k_0 (step 7 in algorithm 1), which is the boundary GT closest to the axis origin (GT_3 in our example denoted as a red triangle). Thus, we can ensure that this GT will be served by MBS_1. Then, the MBS position is refined by covering k_0 and as many boundary GTs as possible within the radius limitation (step 9

in algorithm 1). Those boundary GTs served can be added to the set ρ_{prio}, which refers to the prioritized GTs to be covered. In our example those ones are GTs 2, 3 and 4 (GT_1 is not covered in this iteration as the coverage radius exceeds the maximum one. The next step is to cover those prioritized GTs ρ_{prio} and as many inner GTs as possible (step 10 in algorithm 1). In our example, those inner GTs served are 7 and 8, while GT_9 is not served in this iteration due to the coverage limitation. Finally, the end position of MBS_1 is denoted by the green cross, in the center of the disk of radius R_1. Once the first MBS is placed, we can redefine the sets. We add to the covered subset all those GTs served in the iteration by $\mathcal{K}_C \cup \mathcal{K}_1$, where $\mathcal{K}_1$ stands for the set of GT served by MBS_1. On the other hand, we can update the uncovered set as $\mathcal{K}_U = \mathcal{K}_U \setminus \mathcal{K}_1$.

Once the first MBS is placed the convex hull is updated to link all the boundary GTs of the updated uncovered GTs set. In our example, this will lead to a direct link between GTs 1 and 5. Following the CCW criteria to pick the next boundary GT from the last iteration, $k_0^{'}$, which in this case is GT_5. Then, we update k_0 to $k_0^{'}$ and the previous steps are repeated. Once all GTs are served, the process stops.

We can focus now in the Local Cover algorithm used to place the MBS. This algorithm is taking care to refine the m-th MBS position $\mathbf{u}_m$ given the prioritized set ρ_{prio} including the boundary GTs within the target area and the secondary set ρ_{sec} including the uncovered inner GTs. This problem can be formulated as the following optimization problem

$$\min_{\mathbf{u}_m,\ m\in\mathcal{M}} \quad |\mathcal{K}_m| \quad \text{s. t} \quad \begin{cases} \Phi_1 : \|\mathbf{w}_k - \mathbf{u}_m\| \leqslant d_m \quad \forall\, k \in \mathcal{K}_m \\ \Phi_2 : \mathcal{K}_m \cup \rho_{prio},\ \mathcal{K}_m \subseteq \rho_{sec} \\ \Phi_3 : r_m \leqslant R_{max} \\ \Phi_4 : \gamma_{o,k} \geqslant \gamma_{o,min} \qquad \forall\, k \in \mathcal{K}_m \end{cases} \tag{4.2}$$

where m stands for the current iteration of the spiral algorithm, $\mathbf{u}_m$ is the placement of the target MBS. We have modified the sets restrictions by adding constraint Φ_2. In this case, we have to ensure that all GTs in ρ_{prio} are covered in this iteration, at the same time that we have to cover as much inner GTs as possible from ρ_{sec}. Same than for (4.1), we present algorithm 2 to solve this optimization problem.

Following the explanation supported by the example in figure 4.1, the first step is to reduce the number of GTs to be evaluated in the local cover algorithm as much as possible in order to reduce the computational cost of the algorithm. Thus, it is clear that we can remove all those

GTs at a distance higher than $2R_{max}$ from the boundary GT k_0, as they cannot be served by a single MBS at the same time. For example, in our example GT_3 is guaranteed to be covered by MBS_1. Then, we can draw a red circle centered at GT_3 with radius $2R_{max}$, and exclude all those GTs outside the red circle. Then, at the end the candidates to be covered by MBS_1 are reduced to GTs 1, 2, 3, 4, 7, 8, and 9, which greatly reduces the problem complexity.

The remaining GTs in ρ_{sec} are sorted from closest distance to the current MBS location, and are covered one by one until they cannot be served by the same MBS. In step 4 of algorithm 2, we are moving from ρ_{sec} to ρ_{prio} those GTs already covered, that is within the coverage circle of radius R_m. In our example, once MBS_1 has covered boundary GTs 2, 3 and 4, there is no need to check if GT_7 as it is already covered. Hence, there is no need to solve the 1-center problem in this iteration.

In order to optimally place a MBS given a set of points (step 6 in algorithm 2), we need to solve the 1-center problem, which finds the optimal position for $\mathbf{r}_m$ by minimizing the maximum distance with any point in the set.

Algorithm 2 Local cover algorithm

Input: m-th MBS location $\mathbf{u}_m$, boundary GTs ρ_{prio}, inner GTs ρ_{sec}.

Output: m-th MBS refined location $\mathbf{u}_m$, the coverage radius R_m, covered GTs ρ_{prio}.

procedure [$\mathbf{u}_m$, R_m, ρ_{prio}] = LOCAL_COVER($\{\mathbf{w}_k\}$, ρ_{prio}, ρ_{sec})
  while $\rho_{sec} \neq \varnothing$ **do**
    Update ρ_{sec} removing far GTs ($r > 2R_{max}$) from any GT in ρ_{prio}.
    Move from ρ_{sec} to ρ_{prio} those GTs close ($r < R_m$) to $\mathbf{r}_m$.
    Sort ρ_{sec} from closest distance to $\mathbf{r}_m$.
    Cover first GT k_1 by refining $\mathbf{r}_m$ via solving the 1-center problem.
    if $R_m \leqslant R_{max}$ **then** ▷ Check coverage limitation
      Get h_m from the ATG model to guarantee $\mathrm{PL}_{R_m} = \mathrm{PL}_{max}$.
      if $\gamma_{0,k} < \gamma_{0,min} \ \forall k \in \mathcal{K}_C$ **then** ▷ Check interference
        Move k_1 from the sorted set ρ_{sec} to ρ_{prio}.
      else
        Discard k_1 from ρ_{sec}.
      end if
    else
      Exit while.
    end if
  end while
end procedure

In addition, we need to check our constraints to ensure the life of the system. We need to check if the current GT can be covered within the power limitation, that is not exceeding the maximum coverage radius (step 7 in algorithm 2). For a given m-th MBS transmitted power $P_{t,\,m}$, the received power by the k-th GT depends on the path losses experienced in the communication link as

$$P_{r,\,k}\,(dBm) = P_{t,\,m}\,(dBm) - \mathrm{PL}_{m,\,k}\,(dB) \tag{4.3}$$

In order to guarantee a certain QoS at the k-th GT, we can assume that the received power $P_{r,\,k}$ must exceed a certain threshold P_{min}. This is equivalent to saying that the k-th GT is covered if the path losses experienced in the communication link are less or equal a certain path losses threshold, that is $\mathrm{PL}_{m,\,k} \leqslant \mathrm{PL}_{max}$. Then, we can compute the MBS height h_m by solving the path losses equation of the ATG model (3.10) giving that maximum path losses limitation related to the QoS. In addition, we need to check the signal-to-noise and interference ratio (γ_0) of the already covered GTs in order to check if the placement is producing high interference to the neighbors MBS, that is the QoS is guaranteed for every single user. In our case, we are computing that ratio as

$$\gamma_{0,\,k} = \frac{P_{r,\,k}}{P_n + P_i} \tag{4.4}$$

where P_n stands for the noise power and P_i for the interference received. In the worst scenario, where there are not mechanisms to address the interference, we can write the interference level received at the k-th GT as

$$P_{i,\,k,\,max} = \sum_{\substack{\forall\, k' \in \mathcal{K}_C \\ k' \neq k}} P_{r,\,k'} \tag{4.5}$$

Even thought, we can consider that the interference power is negligible when it achieves some minimum value. When all those constraints are checked, we can move the studied GT to the ρ_{prio} set of the covered GTs by the current MBS. If some constraint is not achieved, we discard this GT, which should be served by another MBS.

4.3 Results and discussion

In this section we are going to review the results obtained by solving the spiral placement algorithm. We generated a randomly uniform distributed topology, whose parameters can be found in table 4.1. In addition, some parameters related to the communication link between the k-th GT and the m-th MBS are depicted in 4.2.

Parameter	**Value**
$\mathcal{K}$	100 GTs
Area	10 km^2
R_{max}	400 m
$\gamma_{0,min}$	2.5 dB
L_{max}	80 dB
f_c	2 GHz
Model	Dense-urban

Table 4.1: Scenario parameters.

Parameter	**MBS Value**	**GT value**
$P_{t,max}$ (Transmitter power)	30 dBm	20 dBm
G_t (Transmitter antenna gain)	3 dB	3 dB
F (Noise figure)	4 dB	6 dB
B (Channel bandwidth)	200 kHz	200 kHz

Table 4.2: Devices parameters.

Figure 4.2 shows the placement obtained by solving the optimization problem in (4.1) via algorithms 1 and 2. That topology required a number of 16 MBS to cover every single user. We can see how all GTs are just served by one MBS to avoid interference. The power constraint controls the radius of each cell, which is adjusted to cover the edge user under the γ_0 and L_{max} limitations. We can see how the placement begins from the most boundary GT at $\mathbf{r}_{76} = (143, 296)$ meters from the axis origin. When MBS_1 is placed, the algorithm considers the next uncovered boundary GT CCW. We can clearly see that spiral placement, from the edges of the area to inwards.

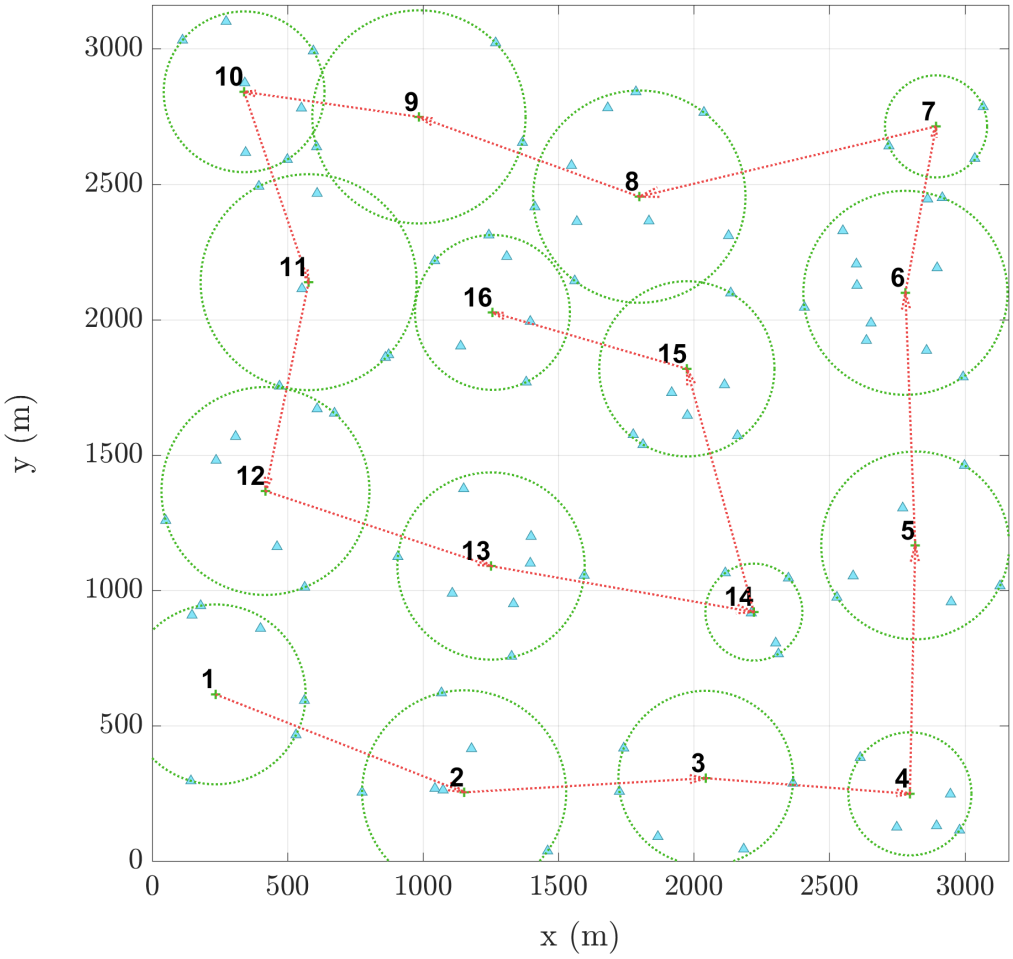

Figure 4.2: Spiral algorithm.

Table 4.3 shows the simulation results in more detail. One can observe that in the studied dense-urban environment the deployment is possible for the maximum height shown in the table. As we have seen in chapter 3, in more detail in figure 3.6, the deployment is possible for all the environments except for the high-rise-urban. In that case, it is not possible to get the maximum path losses available meeting with the obtained coverage radius. This make sense as it is not feasible to get MBS cells of that radius magnitude in this kind of environments, so the radius in this kind of environments should be much smaller, hence the number of MBS deployed increases. Lower MBS heights will lead to a decrease of the path losses impact, which is quite useful for our scenario. Finally, we get the coverage radius that guarantee the $\gamma_{0,min}$ at the edge of the cell, which is lower of the maximum available radius R_{max} due to power limitations.

MBS index m	**MBS position** $\mathbf{u}_m$ (meters)	**MBS radius** R_m (meters)
1	(234, 615, 636)	332
2	(1151, 253, 619)	376
3	(2043, 305, 639)	322
4	(2797, 248, 667)	227
5	(2817, 1165, 631)	346
6	(2780, 2098, 619)	376
7	(2894, 2713, 675)	188
8	(1798, 2454, 613)	391
9	(984, 2748, 612)	393
10	(339, 2841, 648)	296
11	(577, 2138, 610)	398
12	(418, 1366, 616)	383
13	(1251, 1089, 631)	345
14	(2221, 919, 677)	178
15	(1974, 1818, 639)	323
16	(1256, 2026, 651)	285

Table 4.3: Simulation results.

Our updated spiral algorithm has been compared with some other solutions for this placement problem. We have focused the comparison in the first version of the spiral algorithm, but there are other solutions, like a random placement or a placement based on the K-means algorithm. We have realized how our algorithm has improved the benefits of the original spiral algorithm in terms of performance. In the topology of figure 4.2 the number of MBS deployed by the original spiral algorithm is the same ($\mathcal{M} = 16.$) than ours. Otherwise, this results are topology dependant. We have done the experiment for different topologies and we realized that our algorithm behaves quite well, but some times the number of MBS deployed is higher (typically 1 MBS more) than the original spiral algorithm. Anyway, if we focus on the performance of the algorithm for each GT in terms of γ_0, our updated algorithm behaves better. On the other hand, we have compared this placement with a random one, whose deployment values are much higher than ours with high interference among cells, so this solution is not

valid. We have also checked the behaviour of the K-means algorithm in this situation. It needed a larger number of MBS deployed (typically between 4 and 8 MBS more), which is quite higher than the spiral placement, and the interference problem is a critical situation as the number of MBS have been increased and some GTs can be covered by many MBS.

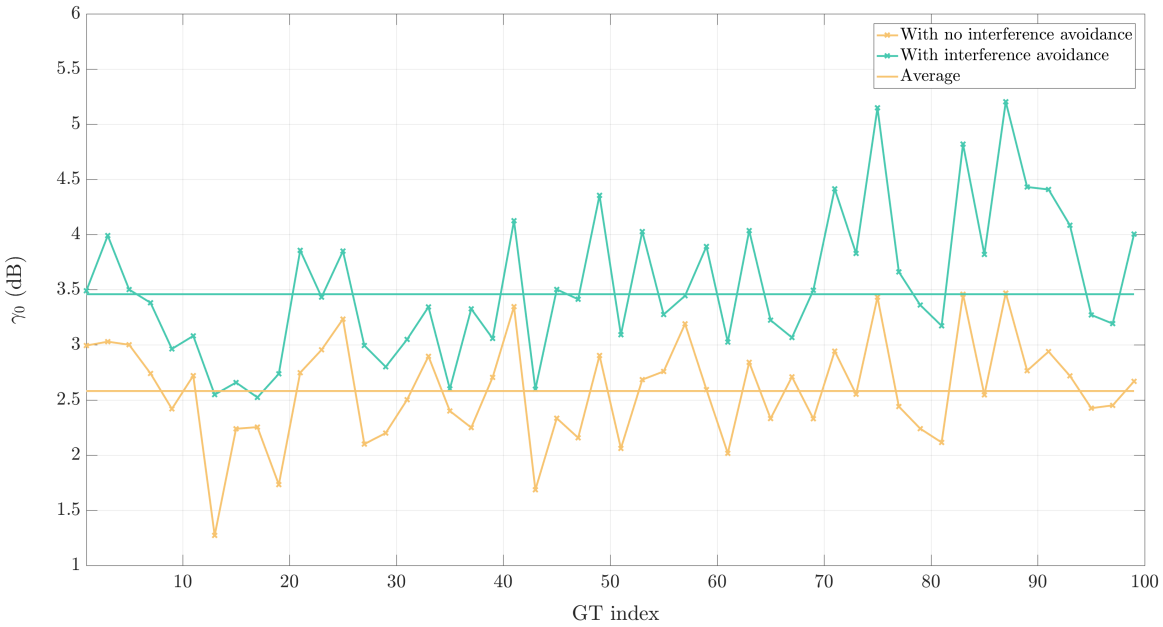

Figure 4.3: γ_0 for a set of GTs.

Figure 4.3 depicts the signal-to-noise and interference γ_0 for every single user in the topology shown in 4.2. We can see how the average γ_0 has increased 1 dB respect to the original spiral algorithm, which is quite an interesting results as we have not compromised the number of MBS deployed to get those results. What is most important in this scenario rather than the average γ_0 is the improvements in critical GTs. For example, GT_{13} has a critical γ_0 without considering the interference constraint, while considering it we have improved his signal in almost 2 dB. We can find many examples for critical GTs, and every one of them have been improved. In fact, the γ_0 value is higher for every single user, there is no GT with lower γ_0 in the updated spiral algorithm.

Once we have made an in deep study of the algorithms performance in one specific topology, we can extend the study for different topologies. The objective is to show that results are not depending on the user distribution in the target area. Figure 4.4 shows the evolution of the MBS cardinality for different increasing GTs density, as well as the signal-to-noise

and interference ratio evolution. This experiment has been done by averaging the results of 1000 random topologies for each one of the GT density scenario. We can see how the MBS cardinality follow the same behaviour for both algorithms until a certain point, where the number of MBS deployed considering the interference increase considerably. This effect is produced because of the need of smaller cells to serve the users without interference. On the other hand, the signal-to-noise and interference ratio has a similar evolution as a counterpart of this cardinality increase. While γ_0 in the first algorithm drops for high density scenarios, the one considering the interference stabilizes at the selected γ_{th}, which in this case is 2.5 dB. Thus, one can find a trade-off between both algorithms depending on the application. Anyway, for emergency scenarios where a certain QoS is necessary to ensure everyone can access the network, the second algorithm responds in a better way if the number of users in the affected area is not huge.

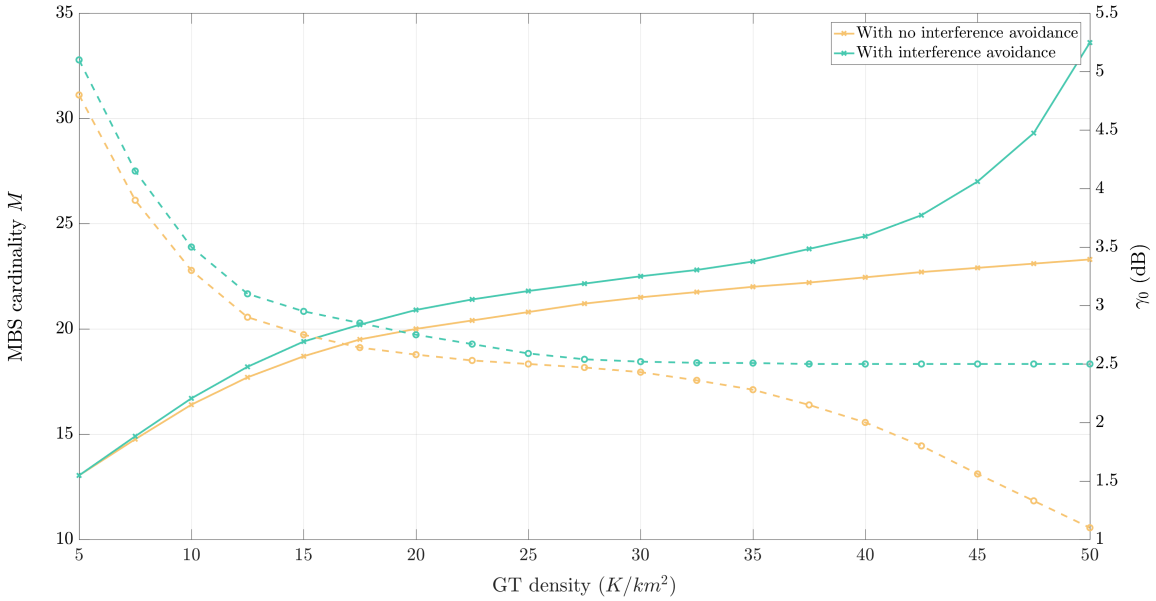

Figure 4.4: MBS deployment and γ_0 for increasing GTs density.

5 | Multiple-access communication

Because of the power limitations in UAV mounted MBS, achieving a high energy efficiency is important. We can optimize the power consumption by focusing the energy to the GT set on the ground, applying beamforming techniques [15]. In this chapter we are going to introduce a novel technique known as non-orthogonal multiple access (NOMA) and see how this technique will be useful for managing properly the power consumption on the MBS side.

5.1 Scenario description

Consider a mmWave-NOMA transmission scenario where the m-th MBS is equipped with an antenna array with P elements, serving GTs equipped with a single antenna. Assume that target GTs for the m-th MBS, denoted with the set $\mathcal{K}_m$ are inside a specific area called *user region*, as shown in figure 5.1.

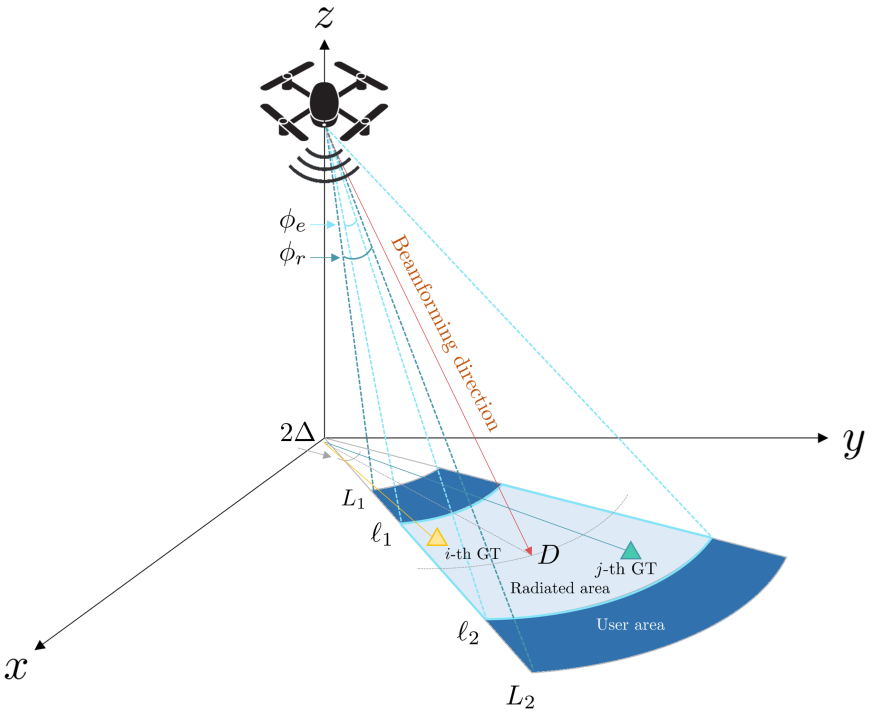

Figure 5.1: MBS beamforming scenario.

We also consider that it is not necessary to fully cover the user region, depending on the distribution of the GTs. Then, from the user region we can find a smaller region called *radiated region*, which is the area covered by the m-th MBS beam. We can characterize the user area by the inner radius L_1, an outer radius L_2, the projected area of the beamwidth on the ground 2Δ. In the same way, the radiated area is characterized by the inner radius ℓ_1, the outer radius ℓ_2 and the same projected beamwidth angle 2Δ.

5.1.1 Coverage

We are going to check the user region coverage for different topologies. We have tried to give consistency to the values chosen in this chapter with the ones used previously. Hence, we are going to set $L_2 = 400$ meters according to the maximum radius chosen before. We have depicted in figure 5.2 the user region coverage in terms of the required vertical angle ϕ_r to cover the user region for different topologies determined by the inner radius L_1.

Note that the vertical beamwidth $\phi_e = 32^\circ$ divides the required vertical beamwidth ϕ_r space into two regions. The upper one stands for the case where $\phi_e < \phi_r$, hence ϕ_e is insufficient to cover the whole user region. On the other hand, the lower region shows the case when the full user region is covered, that is $\phi_e > \phi_r$.

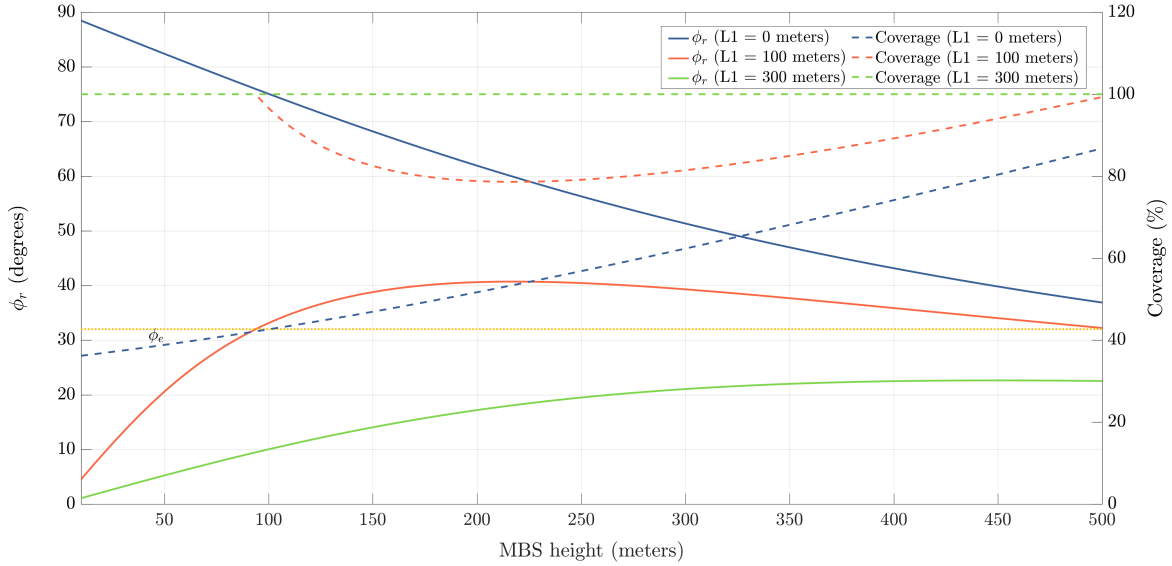

Figure 5.2: MBS beamforming coverage.

In the case of $L_1 = 0$ meters, we are covering all the area, from the origin (which in this scenario corresponds to $\mathbf{r}_m = \mathbf{0}$) towards the limit of the cell at $L_2 = R_{max} = 400$ meters.

We can see how the required vertical angle ϕ_r decreases monotonically when the MBS height increases. With the given values, it is not possible to cover the entire user region. If we simplify the coverage by increasing the inner radius to $L_1 = 100$ meters, we can see how ϕ_r first increases at the same time that the MBS heights increases, an then starts to decrease. Because of this effect, it is possible that the whole user region is not totally covered, but anyway the coverage values are quite high. Finally, we made the inner radius much larger to $L_1 = 300$ meters, the required ϕ_r to cover the entire user region becomes small compared to ϕ_e. Thus, the user region is fully covered at any MBS height.

We can conclude that the user region coverage depends on the vertical beamwidth ϕ_e, the GTs positioning on the ground and the MBS height.

5.1.2 Channel model

Considering the MISO scenario described in subsection 5.1.1, the channel vector $\mathbf{h}_{m,\,k}$ between the m-th MBS and the k-th GT of size $(P \times 1)$ can be written as

$$\mathbf{h}_{m,\,k} = \sqrt{P} \sum_{n=1}^{N_{paths}} \frac{\alpha_{m,\,k,\,n}\, \mathbf{a}_m(\theta_{m,\,k,\,n})}{\sqrt{\mathrm{PL}_{m,\,k}}} \tag{5.1}$$

where N_{paths} stands for the number of multipaths, $\alpha_{m,\,k,\,n}$ is the complex gain of the n-th path and $\theta_{m,\,k,\,n}$ is the angle-of-departure (AoD) of the the n-th path. We can also define the steering vector $\mathbf{a}_m(\theta_{m,\,k,\,n})$ for a uniform linear array (ULA), given by

$$\mathbf{a}_m(\theta_{m,\,k,\,n}) = \frac{1}{\sqrt{P}} \Big[\; 1 \quad \exp\left[-j2\pi \frac{d}{\lambda} \cos\theta_{m,\,k,\,n}\right] \quad \ldots \quad \exp\left[-j2\pi \frac{d}{\lambda}(P-1)\cos\theta_{m,\,k,\,n}\right] \; \Big]^T \tag{5.2}$$

where (d/λ) is the electrical separation within the elements in the array, with d as the distance between them in meters and λ as the wavelength. Thus, the total length of the array can be written as $L = P \times d/\lambda$. Figure 5.3 shows the distribution and the notation for a ULA. The path losses in 5.1 follow the expression defined in 3.10. As the LoS rays have typically more energy than the NLoS ones in ATG links for most of the scenarios, we can simplify the expression in 5.1 by just selecting the LoS path. Hence, the channel expression becomes

$$\mathbf{h}_{m,\,k} = \sqrt{P} \frac{\alpha_{m,\,k}\, \mathbf{a}_m(\theta_{m,\,k})}{\sqrt{\mathrm{PL}_{m,\,k}}} \tag{5.3}$$

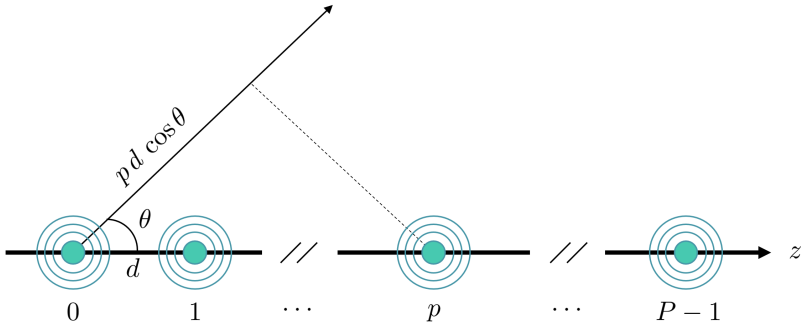

Figure 5.3: Uniform Linear Array.

5.2 NOMA transmission

In this section we are going to study the application of the non-orthogonal multiple access (NOMA) technique in ATG communications. We consider this NOMA transmission to serve multiple users at the same time, using a single down-link (DL) beam, as depicted in figure 5.4.

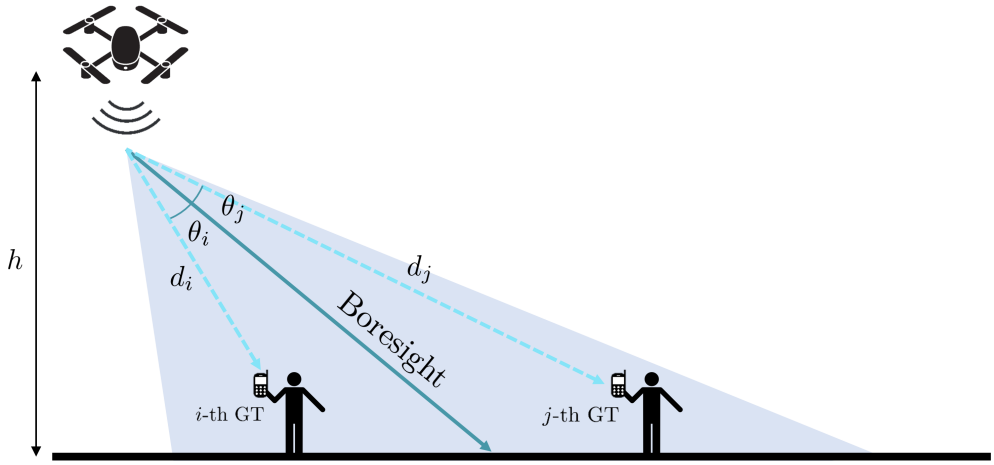

Figure 5.4: NOMA scenario.

5.2.1 NOMA basics

NOMA technique can be the future radio access for 5G networks. Nowadays, all cellular networks are implementing orthogonal multiple access (OMA) techniques, such as time division multiple access (TDMA), frequency division multiple access (FDMA) or code division multiple access (CDMA). None of this techniques can meet the demands for the future radio access systems.

NOMA provides a new dimension to operate, power, as shown in figure 5.5. This technique uses superposition coding at the transmitter such that the successive interference cancellation (SIC) at the receiver can separate the users signals.

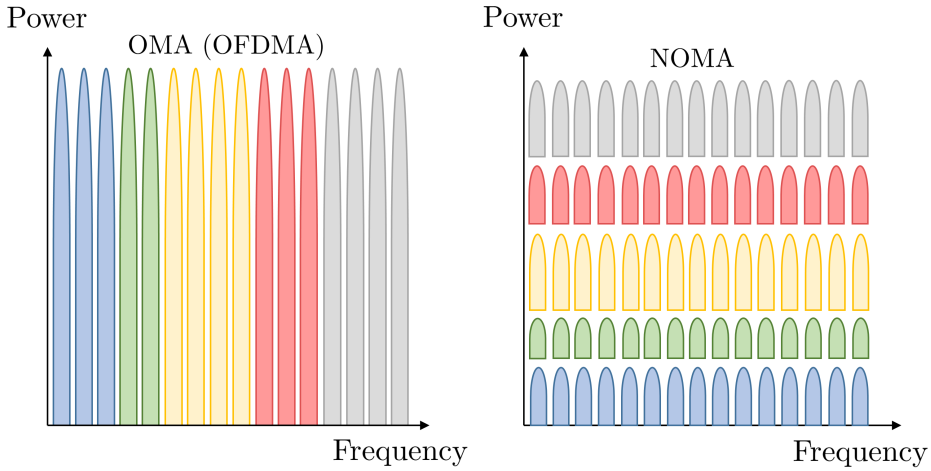

Figure 5.5: OMA and NOMA schemes.

On the transmitter side, which in the case of downlink communications is the MBS, a combined signal as a superposition of the desired signals for the multiple users with different power coefficients is sent to all GTs. On the receiver side, the k-th GT successive interference cancellation (SIC) makes possible to use the same spectrum for all GTs. SIC decodes the signals one by one until the desired one is found. The success of SIC depends on the perfect cancellation of the signals, which is not obvious.

5.2.2 MBS NOMA DL

Power coefficients are allocated n proportional according to their channel conditions. The GT with a bad channel condition, typically the furthest from the MBS, is allocated higher transmission power than another one with better channel conditions. Each GT decodes the strongest signal first, and then substracts the decoded one from the received signal. SIC iterates this process until it finds its own signal. Hence, the GT with the worst channel conditions will be allocated with the highest coefficient, so it will decode its own signal first. This methodology is depicted in figure 5.6.

To order GTs for NOMA transmission to allocate the power coefficients, we consider effective channel gains, which are calculated with respect to the beam $\mathbf{b}_m = \mathbf{a}_m(\bar{\theta}_m)$ transmitted by the m-th MBS, where $\bar{\theta}_m \in \{0, 2\pi\}$ stands for the AoD of the beam $\mathbf{b}_m$. When the beam is

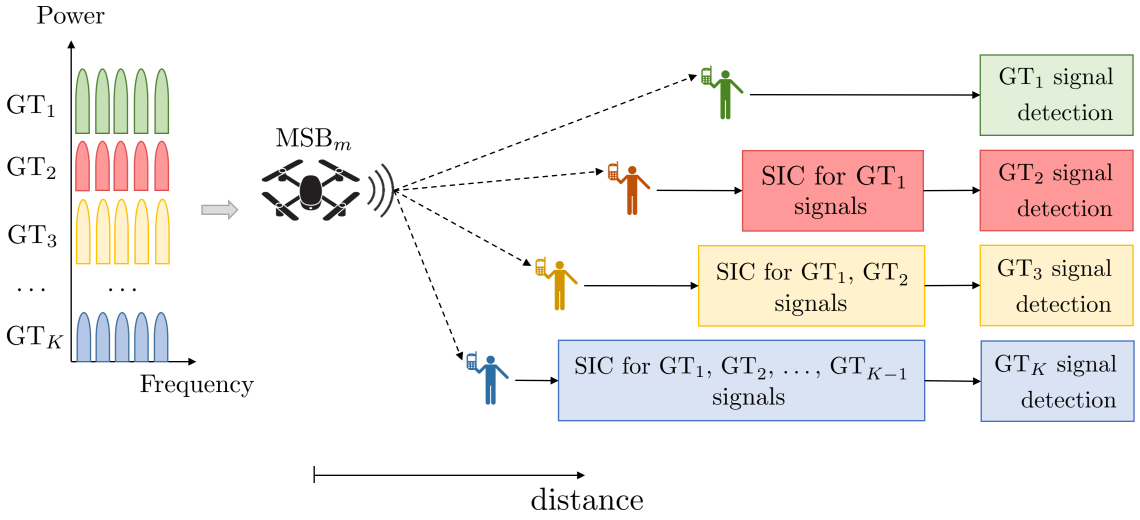

Figure 5.6: MBS NOMA DL for K GTs.

generated, the users within the user region are asked to measure their effective channel gain $|\mathbf{h}_{m,k}^H \mathbf{b}_m|^2$, given by

$$|\mathbf{h}_{m,k}^H \mathbf{b}_m|^2 = P \frac{|\alpha_{m,k}|^2 \, |\mathbf{b}_m^H \mathbf{a}_m(\theta_{m,k})|^2}{\mathrm{PL}_{m,k}} = \frac{P \, |\alpha_{m,k}|^2}{\mathrm{PL}_{m,k}} \left| \frac{\sin\left(\frac{\pi P(\sin\bar{\theta}_m - \sin\theta_{m,k})}{2}\right)}{P \sin\left(\frac{\pi(\sin\bar{\theta}_m - \sin\theta_{m,k})}{2}\right)} \right|^2 \tag{5.4}$$

Then, this effective channel gain is fed back to the MBS, which are ordered as follows

$$|\mathbf{h}_{m,1}^H \mathbf{b}_m|^2 \leqslant \cdots \leqslant |\mathbf{h}_{m,K}^H \mathbf{b}_m|^2 \tag{5.5}$$

where it is assumed that the GT set $\mathcal{K}$ is ordered from the worst channel to the best. Hence, the power allocation of the GTs for the m-th MBS can be ordered as $\beta_{m,1} \geqslant \cdots \geqslant \beta_{m,K}$, where the sum of the total allocations is unitary. Once the power allocation is known in the m-th MBS side, it generates the DL signal $\mathbf{x}_m$ and can be written as

$$\mathbf{x}_m = \sqrt{P_{t,m}} \mathbf{b}_m \sum_{k=1}^{K} \beta_{m,k} \, s_{m,k} \tag{5.6}$$

where $P_{t,m}$ stands for the transmit power of the m-th MBS and $s_{m,k}$ stands for the information of the k-th GT.

Then, the received observation on the k-th GT is

$$y_k = \mathbf{h}_{m,\,k}^H \, \mathbf{x}_m + w_k = \sqrt{P_{t,\,m}} \mathbf{h}_{m,\,k}^H \mathbf{b}_m \sum_{k=1}^{K} \beta_{m,\,k} \, s_{m,\,k} + w_k \tag{5.7}$$

where w_k is zero mean complex additive Gaussian noise with variance $\sigma^2 = N_0$, that is $w_k \sim CN(0, N_0)$.

Signal-to-noise and interference

By using (5.7), we can write the signal-to-noise and interference γ_0 of the i-th GT to detect the j-th GT, with $j < i$ and $j \neq K$, as

$$\gamma_{0,\,j \to i} = \frac{P_{t,\,m} |\mathbf{h}_{m,\,i}^H \mathbf{b}_m|^2 \beta_{m,\,j}^2}{P_{t,\,m} \sum\limits_{l=j+1}^{K} |\mathbf{h}_{m,\,i}^H \mathbf{b}_m|^2 \beta_{m,\,k}^2 + N_0} \tag{5.8}$$

Thus, the resulting signal-to-noise and interference of the i-th GT is given by

$$\gamma_{0,\,i} = \frac{P_{t,\,m} |\mathbf{h}_{m,\,i}^H \mathbf{b}_m|^2 \beta_{m,\,i}^2}{(1 - \delta_{kK}) P_{t,\,m} \sum\limits_{l=i+1}^{K} |\mathbf{h}_{m,\,i}^H \mathbf{b}_m|^2 \beta_{m,\,k}^2 + N_0} \tag{5.9}$$

where δ_{kK} is the Kronecker delta function taking 1 if $k = K$ and 0 otherwise. Hence, the signal-to-noise and interference for the K-th GT with worst channel conditions is

$$\gamma_{0,\,K} = \frac{P_{t,\,m} |\mathbf{h}_{m,\,K}^H \mathbf{b}_m|^2 \beta_{m,\,K}^2}{N_0} \tag{5.10}$$

Data rate

With the signal-to noise and interference expressions in (5.9) and (5.10), we can easily get the total data rates. The DL data rate achievable for the i-th GT can be expressed as

$$R_i^{\text{NOMA}} = \log_2(1 + \gamma_{0,\,i}) \tag{5.11}$$

In addition, the sum rate of the DL communication can be written as

$$R^{\text{NOMA}} = \sum_{k=1}^{K} \log_2(1 + \gamma_{0,\,k}) \xrightarrow[\gamma_0 \uparrow\uparrow]{} \log_2(\gamma_{0,\,K}) \tag{5.12}$$

Outage probability

Assume that the m-th sends information at a rate R_m^{NOMA}. Then, the i-th GT is said to be in outage if $R_i^{\text{NOMA}} < R_m^{\text{NOMA}}$. Then, we can define the outage probability as

$$\text{P}_{\text{OUT},i} = \text{P}\left\{\log_2\left(1 + \frac{P_{t,m}|\mathbf{h}_{m,i}^H \mathbf{b}_m|^2}{N_0}\right) < R_m^{\text{NOMA}}\right\} \tag{5.13}$$

5.2.3 Results and discussion

For the sake of simplicity, in this section we have considered a user region with two users, that is GTs $i = 1$ and $j = 2$. We are going to analyze the rate boundaries for these two users.

Data rate pairs

Figure 5.7 shows the boundaries of the achievable data rate for both NOMA and OMA (in this case we are using OFDMA) transmissions for a symmetric scenario, that is both users have the same signal-to-noise and interference ratio, which is what we are trying to achieve with our study. In this example, both users have a signal-to-noise and interference ratio of $\gamma_{0,1} = \gamma_{0,2} = 3$ dB, according to the results in chapter 4.

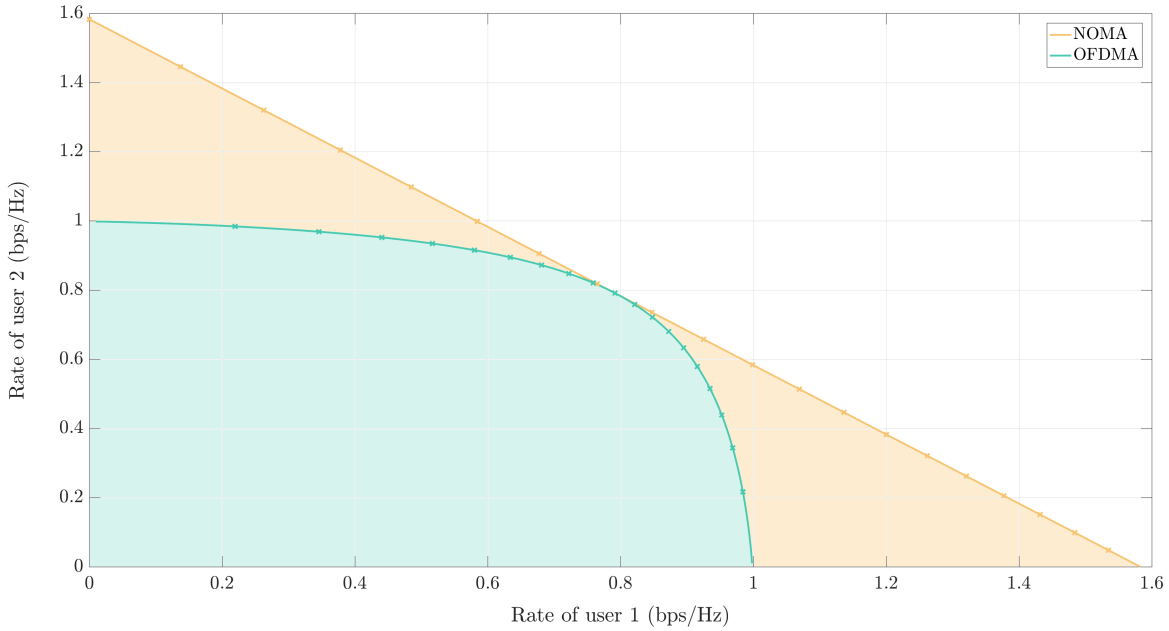

Figure 5.7: NOMA and OMA data rates regions.

We can see how NOMA data rates pair are higher than the ones achieved with OFDMA, except on the corners, where the rates are equal to the single user capacities. When the system is fair, both users experience the same data rate of 0.8 bits per channel use (BPCU). However, when the fairness of the system is not optimal, individual throughput and total capacity are higher with NOMA. Finally, if we reduce the fairness of the system the difference between both techniques becomes much larger.

Imperfect cancellation in SIC

Figure 5.8 depicts the effect of imperfect signal cancellation in SIC. We have analyzed the impact imperfect cancellation by means of an error term ϵ for different values. That means, for instance when $\epsilon = 5\%$, GT_1 can not cancel properly the signal intended for GT_2, and 5% of the power of the second users remains as interference. We can see how this parameters is critical, so the succeed of NOMA highly depends on the perfect signal cancellation.

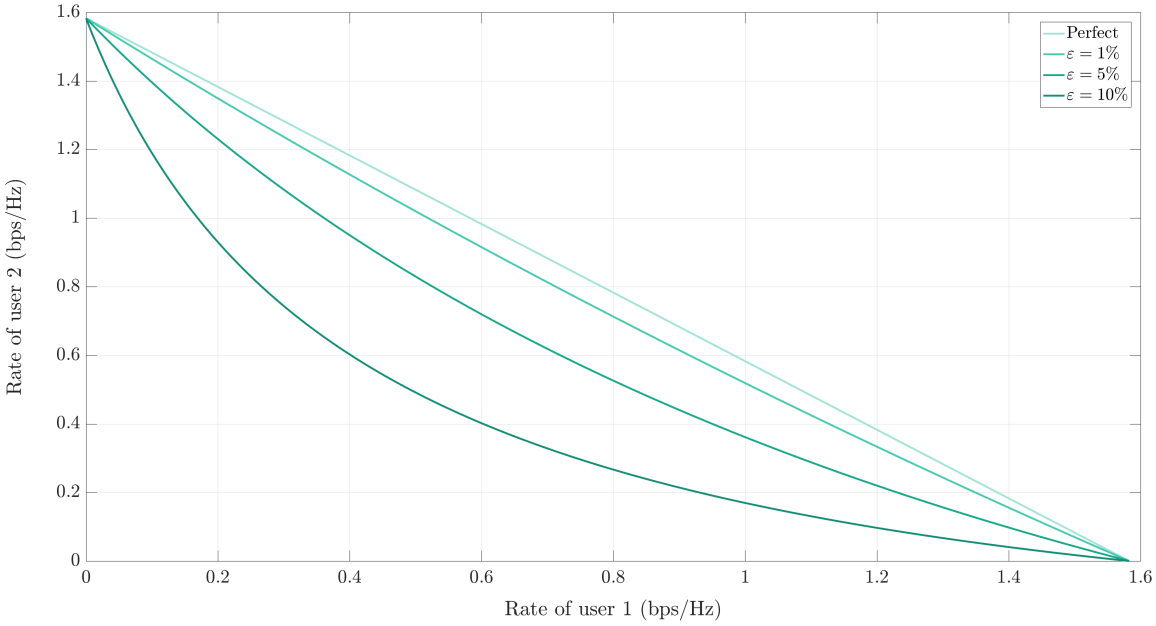

Figure 5.8: Imperfect signal cancellation in SIC.

6 | Conclusions and Future Work

6.1 Conclusions

The main objective of this thesis has been to develop a technique to optimize the deployment of MBS, paying special attention on the placement and the multiple-access technique to fulfill the requirements. We have proposed a system model summarizing our problem scenario by presenting a proper nomenclature followed during all the thesis.

Before the deployment, we made an in deep study on the propagation model between a ground user GT and an aerial platform MBS at a certain height. We used a very known model called air-to-ground (ATG) path losses. We demonstrated how this model makes sense in our scenario by carrying some simulations of the path losses in terms of realistic MBS coverage radius and altitude. By a comparison between the MBS height and the radius to fulfill a certain QoS requirement we realized that there is an maximum coverage radius for each urban environment under study, so increasing the altitude of the MBS do not lead to higher coverage regions under the same QoS conditions.

When the knowledge of the propagation model is fulfilled, we focused on the placement problem. This problem is not trivial and there is an extended literature about this topic. In our scenario, we considered as the optimal placement as the lower number of MBS deployed in the field by maximizing the coverage of all users in the target area. We based our work on a spiral algorithm and improve it by adding more realistic and useful constraints, as the interference avoidance between MBS. We simulated our algorithm and get interesting results, improving the ones obtained with the previous version of the spiral algorithm.

Finally, once the placement problem has been addressed, the communication between the GTs and the MBS had to be tackled. We made an study of the multiple-access techniques in ATG communications by applying beamforming to the user areas. In UAV based MBS is very important to optimize the power consumption because of its limitations. In order to optimize the performance with the received signal-to-noise and interference on the GT, we purposed the NOMA technique in front of the well known OMA techniques to get better data rates under the same conditions.

6.2 Future work

This thesis considers the problem of optimizing the deployment of MBS in a certain area in emergency scenarios, where the coverage for all the users has to be guarantied.

One interesting research line to follow is to consider the same deployment conditions in terms of coverage maximization and interference minimization by means of moving GTs. This should lead to an adaptive MBS placement bounded to the GTs path planning. Machine learning algorithms can be applied to predict the movement of the GTs and plan an optimal trajectory of the MBS already deployed.

On the other hand, the problem can be relaxed by considering more flexibility in some of the constraints. If we let the system to be unfair with users with poor conditions, the results achievable considerably increase. We have seen how the number of MBS deployed with the interference avoidance constraint grows exponentially for dense areas. In this kind of scenarios other interference avoidance techniques such as channel coding are needed. Despite that, the signal-to-noise and interference ratio is above the thershold one in this last case, so some applications may be interested more in QoS rather than the number of MBS deployed, or the other way around. It is possible to find a trade-off merging both ideas to find the optimal solution for a certain application.

Another approach of the problem could consist on a reuse of the algorithm for other kind of scenarios. Imagine a sensor network getting periodically measurements. In this case the sensors are the GTs in our system model. This system is not critical in terms of latency, and data can be collected once in a while. The idea can be to deploy just one UAV following the spiral path along all the users to collect the data. In addition, the transmitter power is controlled in each spot of the path according to the coverage radius of the algorithm. Hence, it is possible to collect the data of all the users with just one MBS deployment. Moreover, this problem can be relaxed for another kind of networks where the latency is quite important. Hence, a fewer number of MBS can be deployed, and each one of them can follow a trajectory between some of the spots in the spiral path, going and coming back all the time.

Finally, the communication problem can be extended to other techniques applying the same beamforming criteria to reduce the power consumption. It can be also interesting to extend the work by evaluating the outage probability of our system, finding the enhancements with the first version. This is a hot topic in the literature, as the problem is quite novel.

References

[1] Q. Wu, L. Liu, and R. Zhang, "Fundamental trade-offs in communication and trajectory design for UAV-enabled wireless network", in IEEE Wireless Communications Magazine, vol. 26, no. 1, pp. 36-44, February 2019.

[2] X. Cao, P. Yang, M. Alzenad, X. Xi, D. Wu and H. Yanikomeroglu, "Airborne Communication Networks: A Survey", in IEEE Journal on Selected Areas in Communications, vol. 36, no. 9, pp. 1907-1926, September 2018.

[3] N. Zhao, W. Lu, M. Sheng, Y. Chen, J. Tang, R. Yu, and K. Wong, "UAV-assisted emergency networks in disasters", in IEEE Wireless Communications Magazine, vol. 26, no. 1, pp. 45-51, February 2019.

[4] R. Singh, M. Thompson, S. Mathews, O. Agbogidi, K. Bhadane, and K. Namuduri, "Aerial Base Stations for enabling cellular communications during emergency situation", in 2017 International Conference on Vision, Image and Signal Processing (ICVISP), pp. 103-108, September 2017.

[5] Y. Zeng, R. Zhang, and T. J. Lim, "Wireless Communications with Unmanned Aerial Vehicles: Opportunities and Challenges", in IEEE Communications Magazine, vol. 54, no. 5, pp. 36-42, May 2016.

[6] A. Al-Hourani, S. Kandeepan, and S. Lardner, "Optimal LAP Altitude for maximum coverage", in IEEE Wireless Communications Letters, vol. 3, no. 6, pp. 569-572, July 2014.

[7] C. Lai, C. Chen, and L. Wang, "On-Demand Density-Aware UAV Base Station 3D Placement for Arbitrarily Distributed Users With Guaranteed Data Rates", in IEEE Wireless Communications Letters, vol. 8, no. 3, pp. 913-916, April 2019.

[8] B. Galkin, J. Kibilda, and A. DaSilva, "Deployment of UAV-mounted access points according to spatial user locations in two-tier cellular networks", in I2016 Wireless Days (WD), pp. 1-6, March 2016.

[9] M. Alzenad, A. El-Keyi, F. Lagum, and H. Yanikomeroglu, "3-D Placement of an Unmanned Aerial Vehicle Base Station (UAV-BS) for Energy Efficient Maximal Coverage", in IEEE Wireless Communications Letters, vol. 6, no. 4, pp. 434-437, August 2017.

[10] M. Alzenad, A. El-Keyi, F. Lagum, and H. Yanikomeroglu, "3-D Placement of an Unmanned Aerial Vehicle Base Station (UAV-BS) for Maximum Coverage of Users WIth Different QoS Requirements", in IEEE Wireless Communications Letters, vol. 7, no. 1, pp. 38-41, February 2018.

[11] J. Lyu, Y. Zeng, R. Zhang, and T. J. Lim, "Placement Optimization of UAV-Mounted Mobile Base Stations", in IEEE Communications Letters, vol. 21, no. 3, pp. 604-607, March 2017.

[12] P. Agarwal, and M. Procopiuc, "Exact and approximation algorithms for clustering", in Proc. 9th Annu. ACM-SIAM Symp. Discrete Algorithms, pp. 656-667, January 1998.

[13] N. Megiddo, and J. Supowit, "On the complexity of some common geometric location problems", in SIAM J. Comput., vol. 13, no. 1, pp. 182-196, March 1984.

[14] I. Bor-Yaliniz, M. Salem, G. Senerath, and H. Yanikomeroglu, "Is 5G Ready for Drones: A Look into Contemporary and Prospective Wireless Networks from a Standardization Perspective", in IEEE Wireless Communications Magazine, vol. 26, no. 1, pp. 18-27, February 2019.

[15] N. Rupasinghe, Y. Yapici, I. Güvenç, and Y. Kakishima, "Non-Orthogonal Multiple Access for mmWave drones with Multi-Antenna transmission", in IEEE Transactions on Communications, vol. 67, no. 1, pp. 762-777, January 2017.

[16] M. Sohail, C. Yen, and S. Won, "Non-Orthogonal Multiple Access for Unmanned Aerial Vehicle Assisted Communication", in IEEE Access, vol. 6, pp. 22716-22727, June 2018.

[17] N. Rupasinghe, S. Ibrahim, and I. Güvenç, "Optimum Hovering Locations with Angular Domain User Separation for Cooperative UAV Networks", in 2016 IEEE Global Communications Conference (GLOBECOM), pp. 1-6, December 2016.

[18] L. Wang, Y. Che, J. Long, L. Duan, and K. Wu, "Multiple Access MmWave Design for UAV-Aided 5G Communications", in IEEE Wireless Communications Magazine, vol. 26, no. 1, pp. 64-71, February 2019.

A | Time planning

Figure A.1 shows the Gantt diagram of the master's thesis. For an accurate explanation of each work-package, we refer to section 1.1.1.

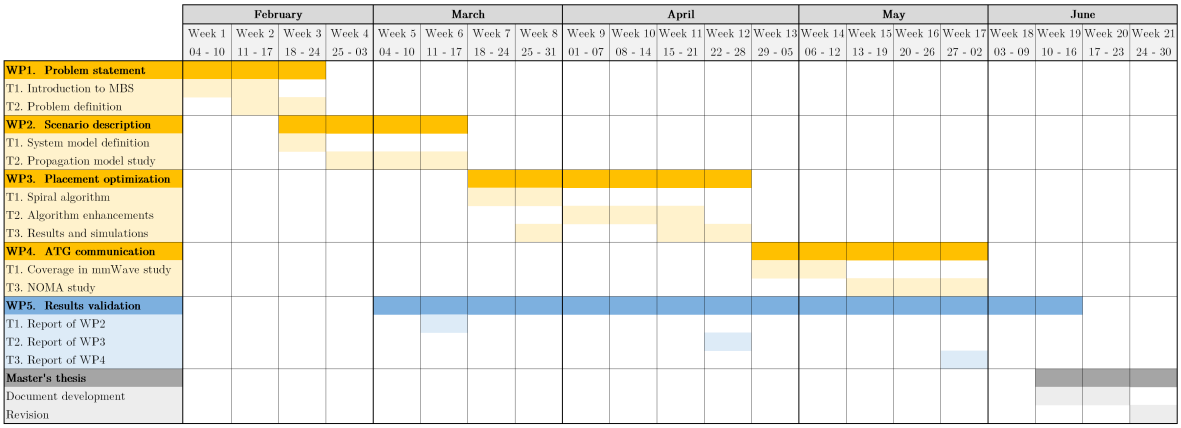

Figure A.1: Time planning of the master's thesis.

Note that during all along the project an autonomous study is needed in order to a suitable development of the work.

B | Poster related

Find attached on the next page a poster related to this work. This poster was presented on the Open Day of the Centre for Telecommunication Research (CTR) at the Department of Informatics in King's College London (KCL) on the 4th of June 2019. During the day, some conferences took place from professors from KCL and University of Bristol, at the same time some companies came to review the current technologies and the further future, such as British Telecom (BT). Finally, some demos and posters presentations where done.

Optimal placement of Mobile Base Stations for maximum coverage

Research group: David Grau, Toktam Mahmoodi

email: david.grau_marina@kcl.ac.uk, toktam.mahmoodi@kcl.ac.uk

KING'S College LONDON

Research scenario

Mobile Base Stations (MBS) can provide wireless services in a variety of scenarios. This work is focused in the case of terrestrial Base Stations (BS) failure, where MBS can be easily and rapidly deployed to serve the demands of each Ground Terminal (GT) in the target area.

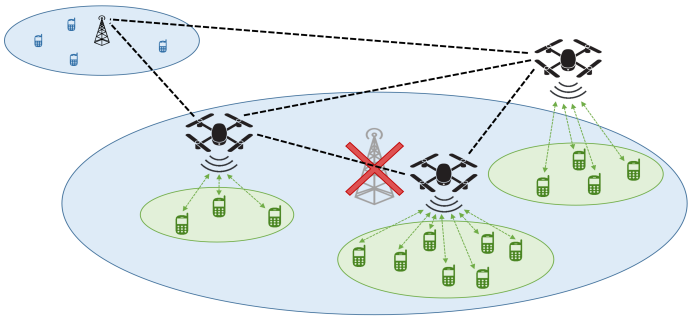

Challenges

- **MBS positioning** - find the optimal 3-D MBS position.
- **Maximum coverage** - maximize the number of GT covered by a single MBS.
- **QoS guarantee** - provide good service to each GT.
- **System life** - minimize MBS power consumption.
- **Cost reduction** - minimize the number of MBS deployed.

Air-to-ground model

The model combines line-of-sight (LoS) and non line-of-sight (NLoS) signals in different environments. Following this criteria, there is a maximum MBS height to provide a certain QoS, in terms of the cell radius. Increasing the MBS height leads to larger path losses due to scattering and fading.

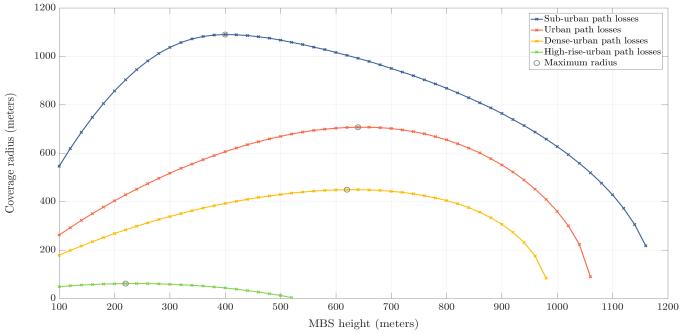

Spiral algorithm

The problem formulation can be resumed as an optimization problem,

$$\min_{\substack{\{\mathbf{u}_m\},\ m\in\mathcal{M}\\ \{\gamma_{o,k}\},\ k\in\mathcal{K}}} \quad |\mathcal{M}| \quad \text{s.t} \quad \begin{cases} \Phi_1: \min\limits_{m\in\mathcal{M}} \|\mathbf{w}_k - \mathbf{u}_m\| \le d_m \\ \Phi_2: r_m \le R_{max} \\ \Phi_3: \gamma_{o,k} \ge \gamma_{o,min} \end{cases}$$

where $\mathcal{M}$ stands for the cardinality of the MBS set. Hence, the number of MBS deployed is minimized. In order to perform the deployment, we solve the optimization problem following an spiral algorithm.

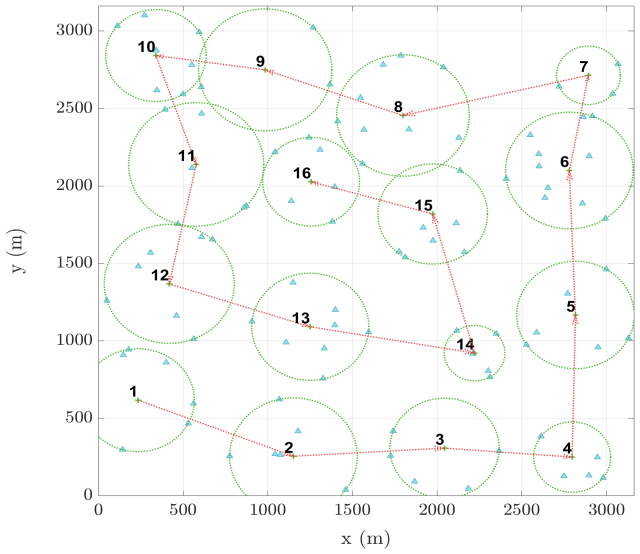

This figure shows the MBS deployment in a certain area with 100 users uniformly and randomly distributed within a certain area. Note how the power budget is controlled at MBS level, where the radius of the cell is set to give a certain QoS to the edge user.

References

J. Lyu, Y. Zeng, R. Zhang, and T. J. Lim, "Placement Optimization of UAV-Mounted Mobile Base Stations", in IEEE Communications Letters, vol. 21, no. 3, pp. 604-607, March. 2017.

M. Alzenad, A. El-Keyi, C. Soria and H. Yanikomeroglu, "3-D Placement of an Unmanned Aerial Vehicle Base Station (UAV-BS) for Energy Efficient Maximal Coverage", in IEEE Wireless Communications Letters, vol. 6, no. 4, pp. 434-437, Aug. 2017.

X. Cao, P. Yang, M. Alzenad, X. Xi, D. Wu and H. Yanikomeroglu, "Airborne Communication Networks: A Survey", in IEEE Journal on Selected Areas in Communications, vol. 36, no. 9, pp. 1907-1926, Sep. 2018.